

METHODOLOGICAL NOTES

PACS numbers: 42.25.Bs, **62.20. – x**, 78.20.Fm

Acoustics and optics of absorptive crystals: a universal formalism for topological effects

V I Alshits, V N Lyubimov

DOI: 10.3367/UFNe.0183.201310j.1123

Contents

Abstract. A universal form of the equations for acoustical and optical wave fields in absorptive crystals is obtained. On this basis, a unified formalism is constructed and used to describe the effect of absorption on the topology of polarization fields and wave surfaces of elastic and electromagnetic waves close to conical acoustic and optical axes. Unless forbidden by symmetry, both types of axes are split by absorption, with the consequences that the wave surfaces acquire self-intersection lines connecting pairs of split axes and that new singular points with the Poincaré indices $n = \pm 1/4$ arise in the polarization fields. Near the split points, the waves of degenerate branches show an abrupt increase in ellipticity, which transforms the internal conical refraction from a local property along the degeneracy direction into a continuum phenomenon occurring throughout this entire region. For each direction of the wave normal, there is a universal refraction cone, the same as for zero absorption. The ends of ray velocity vectors move along the universal section of this cone. This section is elliptic in acoustics and circular in optics. The kinematics of this precession depend in an essential way on the direction of the wave normal.

V I Alshits, V N Lyubimov Shubnikov Institute of Crystallography, Russian Academy of Sciences,
Leninskii prosp. 59, 119333 Moscow, Russian Federation
Tel. +7 (495) 330 82 74. Fax +7 (499) 135 10 11
E-mail: alshits@ns.crys.ras.ru, lyubvn36@mail.ru

Received 11 February 2013, revised 28 May 2013
Uspekhi Fizicheskikh Nauk **183** (10) 1123 – 1140 (2013)
DOI: 10.3367/UFNr.0183.201310j.1123
Translated by M Sapozhnikov; edited by A M Semikhatov

1. Introduction

Equations determining the structure of waves in the optics and acoustics of crystals are essentially different. Electromagnetic waves are described by the Maxwell equations [1–4], while elastic waves are described by the Christoffel equations [5–7]. On the other hand, polarization fields and wave surfaces in the optics and acoustics of crystals near the degeneracy directions of phase velocities give similar topological responses to incorporating the absorption, which, as we see in what follows, allows a unified description.

The influence of absorption on the optical and acoustic properties of crystals does not simply reduce to the trivial attenuation of the wave field during its propagation. Principally new degeneracy directions, so-called singular axes, appear. This occurs due to the splitting of conical optical and acoustic axes, not coinciding with symmetry axes. As the wave normal **m** approaches such singular axes, the wave ellipticity drastically increases and becomes circular at the degeneracy points. On the refraction and absorption surfaces, self-intersection lines connecting the split degeneracy points appear.

The fundamentals of the optics of absorptive crystals are associated with the names Voigt, Drude, and Fedorov (see review [8]). A concise description of the optical properties of absorptive crystals is given in [2–4]. The topological aspects of the problem have also been actively studied in recent decades. In particular, it was shown in [9–11] that split axes define singular points in the complex polarization field corresponding to the topological charge (Poincaré index) $n = 1/4$. In addition, according to [11], at the ends of the self-intersection

wedge of the velocity surface corresponding to degeneracy points, geometric singularities appear in the form of cusps characterized by a flat fan of normals and an infinite curvature. The replacement of a conical contact point by a self-intersection wedge strongly affects the internal conical refraction as well [11].

Similar effects in crystal acoustics were investigated in [12–16]. The inclusion of absorption again leads to the splitting of conical degeneracies into pairs of singular points. The vicinity of the split axes is then characterized by similar geometrical and polarization features [12, 16] and a nontrivial transformation of the properties of internal conical refraction [16].

In this paper, we show that despite all the differences between the master acoustic and optical equations, they can be represented in a unified form thanks to the generality of the wave phenomena in the vicinity of degeneracies. This opens up the possibility of a universal description of the topological characteristics of electromagnetic and elastic waves. We describe not only the known acoustic and optical properties of absorptive crystals but also a number of qualitatively new features of their acoustics and optics, which have never been discussed before.

2. Wave equations in the vicinities of degeneracy directions

In this section, we derive equations describing elastic and electromagnetic waves in an absorptive crystal in the vicinity of the directions of acoustic and optical axes. We see that although the master equations in optics and acoustics are different, plane electromagnetic and elastic waves can be described using a unified mathematical formalism.

2.1 Acoustic equations for absorptive crystals

We consider a viscoelastic medium with an arbitrary anisotropy, described by the elastic modulus tensor $\hat{c} = \{c_{ijkl}\}$, the viscosity tensor $\hat{\eta} = \{\eta_{ijkl}\}$, and the density ρ. The elastic displacement field $\mathbf{u}(\mathbf{r}, t)$ in such a medium is described by the known equation of motion [5]

$$\rho \ddot{u}_i = c_{ijkl}\, u_{l,kj} + \eta_{ijkl}\, \dot{u}_{l,kj}\,, \tag{1}$$

where dots over the function u denote time derivatives, while the derivatives with respect to spatial coordinates are denoted as $\partial/\partial x_k \ldots \equiv \ldots_{,k}$. For an elastic wave

$$\mathbf{u}(\mathbf{r}, t) = C\mathbf{U} \exp\left[\mathrm{i}k(\mathbf{mr} - vt)\right] \tag{2}$$

with the amplitude C, polarization $\mathbf{U}$, wave vector $k = k' + \mathrm{i}k''$, phase velocity v, and frequency $\omega = kv$, Eqn (1) reduces to the generalized Christoffel equation [12, 16]

$$\left[\mathbf{m}(\hat{c} - \mathrm{i}\omega\hat{\eta})\mathbf{m}\right]\mathbf{U} = \rho v^2 \mathbf{U}\,. \tag{3}$$

Equation (3) determines complex polarization vectors $\mathbf{U}_\alpha = \mathbf{U}'_\alpha + \mathrm{i}\mathbf{U}''_\alpha$ and phase velocities $v = v'_\alpha - \mathrm{i}v''_\alpha$ of three eigenwaves ($\alpha = 1, 2, 3$).

When absorption is neglected, the elastic waves of degenerate branches propagating along the acoustic axis $\mathbf{m}_0$ have real polarization vectors $\mathbf{U}$, which can be arbitrarily oriented in the degeneracy plane D orthogonal to the polarization vector $\mathbf{A}_{03}$ of the nondegenerate wave.

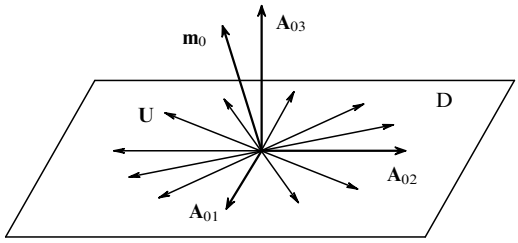

Figure 1. Choice of the basis vectors $\mathbf{A}_{01}$, $\mathbf{A}_{02}$, and $\mathbf{A}_{03}$ in acoustics; $\mathbf{m}_0$ is the direction of the initial acoustic axis and D is the allowed polarization plane in the absence of absorption.

We take two arbitrary unit, mutually orthogonal vectors $\mathbf{A}_{01}$ and $\mathbf{A}_{02}$ in this plane, which together with $\mathbf{A}_{03}$ form an orthogonal basis (Fig. 1). The vectors $\mathbf{A}_{01}$ and $\mathbf{A}_{02}$ enter the key relations of the acoustics of absorptive crystals, their arbitrary choice in the plane D not affecting the invariance of final results.

2.2 Optical equations for absorptive crystals

We consider a nonmagnetic crystal with an arbitrary dielectric anisotropy and weak absorption. We specify an electromagnetic wave propagating in the crystal by its magnetic component

$$\mathbf{h}(\mathbf{r}, t) = C\mathbf{H} \exp\left[\mathrm{i}k(\mathbf{mr} - vt)\right], \tag{4}$$

where the polarization $\mathbf{H}$ and the phase velocity v are defined by the Maxwell equations [2]

$$\mathbf{H} = \frac{1}{v\mu_0}\,\mathbf{m} \times \mathbf{E}\,, \qquad \mathbf{E} = -\frac{1}{v\varepsilon_0}(\hat{\varepsilon}^{-1} - \mathrm{i}\hat{\delta})\mathbf{m} \times \mathbf{H}\,. \tag{5}$$

Here, $\mathbf{E}$ is the polarization of the electric component $\mathbf{e}(\mathbf{r}, t)$ of the wave, $\hat{\varepsilon}^{-1}$ is the inverse permittivity tensor describing the optical properties of the medium in the absence of absorption, $\hat{\delta} = \{\delta_{ij}\}$ is the tensor taking the influence of absorption into account, and μ_0 and ε_0 are the permeability and permittivity of free space. The components of the tensors $\hat{\varepsilon}^{-1}$ and $\hat{\delta}$ are dimensionless: all the physical quantities are written in the SI system, in which the permittivity of a crystal is defined as $\hat{\varepsilon}\varepsilon_0$ and the speed of light in the vacuum is $c = 1/\sqrt{\varepsilon_0\mu_0}$.

Eliminating the electric field $\mathbf{E}$ from (5), we obtain the equation for $\mathbf{H}$:

$$-\mathbf{m} \times \left[(\hat{\varepsilon}^{-1} - \mathrm{i}\hat{\delta})\mathbf{m} \times \mathbf{H}\right] = \left(\frac{v}{c}\right)^2 \mathbf{H}\,, \tag{6}$$

which is

$$-\left\{\mathbf{m}\left[\hat{e}(\hat{\varepsilon}^{-1} - \mathrm{i}\hat{\delta})\hat{e}\right]\mathbf{m}\right\}\mathbf{H} = \left(\frac{v}{c}\right)^2 \mathbf{H} \tag{7}$$

in terms of the Levi-Civita antisymmetric unit tensor $\hat{e} \equiv \{e_{ijk}\}$. Equation (7) specifies velocities v_α and polarization vectors $\mathbf{H}_\alpha$ as eigenvalues and eigenvectors of the corresponding tensor in its left-hand side. Among three eigenvectors, the purely longitudinal polarization vector $\mathbf{H}_3 \parallel \mathbf{m}$ is also present. But we see from (6) that its eigenvalue is $v_3 = 0$. Therefore, the longitudinal solution is static and cannot describe a wave. It is for this reason that electromagnetic waves are always purely transverse ($\mathbf{H}_\alpha \perp \mathbf{m}$), and only two independent isonormal waves can propagate in nondegenerate directions of $\mathbf{m}$.

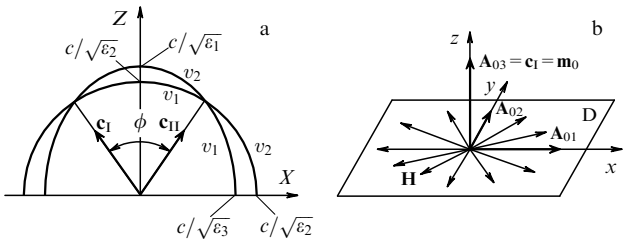

Figure 2. (a) Section of the phase velocity surface $v_{1,2}(\mathbf{m})$ of an optically transparent biaxial crystal. (b) Choice of the $(\mathbf{A}_{01}, \mathbf{A}_{02}, \mathbf{A}_{03})$ basis.

According to [2–4], the real tensor $\hat{\varepsilon}^{-1}$ can be written in the invariant form

$$\hat{\varepsilon}^{-1} = a\hat{I} - b(\mathbf{c}_\mathrm{I} \otimes \mathbf{c}_\mathrm{II} + \mathbf{c}_\mathrm{II} \otimes \mathbf{c}_\mathrm{I}), \qquad \mathbf{c}_\mathrm{I}^2 = \mathbf{c}_\mathrm{II}^2 = 1, \tag{8}$$

where $\hat{I}$ is the unit matrix, $\mathbf{c}_\mathrm{I}$ and $\mathbf{c}_\mathrm{II}$ are the directions of two optical axes of the crystal in the absence of absorption, and the scalars a and b and the vectors $\mathbf{c}_\mathrm{I}$ and $\mathbf{c}_\mathrm{II}$ are expressed in terms of invariant parameters $1/\varepsilon_i$, the eigenvalues of $\hat{\varepsilon}^{-1}$:

$$a = \frac{1}{\varepsilon_2}, \qquad b = \frac{\varepsilon_3 - \varepsilon_1}{2\varepsilon_1\varepsilon_3}, \qquad \mathbf{c}_{\mathrm{I,II}} = (\mp c_1, 0, c_3), \tag{9}$$

$$c_1 = \sin\frac{\phi}{2} = \sqrt{\frac{(\varepsilon_2 - \varepsilon_1)\varepsilon_3}{(\varepsilon_3 - \varepsilon_1)\varepsilon_2}}, \qquad c_3 = \cos\frac{\phi}{2} = \sqrt{\frac{(\varepsilon_3 - \varepsilon_2)\varepsilon_1}{(\varepsilon_3 - \varepsilon_1)\varepsilon_2}}. \tag{10}$$

Here, the indices $i = 1, 2, 3$ of the components ε_i correspond to those in the inequality $\varepsilon_1 < \varepsilon_2 < \varepsilon_3$. In this case, the optical axes of a transparent crystal lie in the XZ plane of the coordinate system $\{X, Y, Z\}$ constructed on the eigenvectors of $\hat{\varepsilon}^{-1}$ (Fig. 2a).

The real phase velocities of isonormal waves in the directions $\mathbf{c}_\mathrm{I}$ and $\mathbf{c}_\mathrm{II}$ coincide, and conic degeneracies appear. In what follows, we take the vector $\mathbf{m}_0 = \mathbf{c}_\mathrm{I}$ as the unperturbed degeneracy direction. Then the degeneracy plane D is orthogonal to the optical axis $\mathbf{c}_\mathrm{I}$. Similarly to the introduction of a basis in the acoustic case (see Fig. 1), it is convenient to introduce the new orthonormalized basis (Fig. 2b)

$$\mathbf{A}_{01} = \frac{(\mathbf{c}_\mathrm{I} \times \mathbf{c}_\mathrm{II}) \times \mathbf{c}_\mathrm{I}}{|\mathbf{c}_\mathrm{I} \times \mathbf{c}_\mathrm{II}|}, \qquad \mathbf{A}_{02} = \frac{\mathbf{c}_\mathrm{I} \times \mathbf{c}_\mathrm{II}}{|\mathbf{c}_\mathrm{I} \times \mathbf{c}_\mathrm{II}|}, \qquad \mathbf{A}_{03} = \mathbf{c}_\mathrm{I} = \mathbf{m}_0, \tag{11}$$

corresponding to the $\{x, y, z\}$ coordinate system rotated with respect to the $\{X, Y, Z\}$ system around the $Y = y$ axis to make the z axis coincident with the $\mathbf{c}_\mathrm{I}$ axis.

2.3 Universal wave equation and its solution in the vicinity of degeneracy directions

We introduce the universal wave

$$\mathbf{a}(\mathbf{r}, t) = C\mathbf{A}\exp\left[\mathrm{i}k(\mathbf{mr} - vt)\right], \qquad \mathbf{a} = \begin{cases} \mathbf{u} & (\mathrm{ac}), \\ \mathbf{h} & (\mathrm{op}), \end{cases} \quad \mathbf{A} = \begin{cases} \mathbf{U} & (\mathrm{ac}), \\ \mathbf{H} & (\mathrm{op}), \end{cases} \tag{12}$$

and generalized material tensors

$$\hat{\Lambda}' = \begin{cases} \dfrac{\hat{c}}{\rho} & (\mathrm{ac}), \\ -c^2\hat{e}\hat{\varepsilon}^{-1}\hat{e} & (\mathrm{op}), \end{cases} \qquad \hat{\Lambda}'' = \begin{cases} \dfrac{\omega\hat{\eta}}{\rho} & (\mathrm{ac}), \\ -c^2\hat{e}\hat{\delta}\hat{e} & (\mathrm{op}), \end{cases} \tag{13}$$

which are simultaneously related to optics (op) and acoustics (ac). In these terms, instead of (3) and (7), we obtain the generalized Christoffel equation for elastic and electromagnetic waves in an absorptive crystal:

$$(\hat{Q}' - \mathrm{i}\hat{Q}'')\mathbf{A} = v^2\mathbf{A}, \qquad \hat{Q}' = \mathbf{m}\hat{\Lambda}'\mathbf{m}, \quad \hat{Q}'' = \mathbf{m}\hat{\Lambda}''\mathbf{m}. \tag{14}$$

As mentioned in Section 2.2, we consider complex phase velocities v_α and elliptic polarizations $\mathbf{A}_\alpha$ ($\alpha = 1, 2, 3$ for acoustics and $\alpha = 1, 2$ for optics):

$$v_\alpha = v'_\alpha - \mathrm{i}v''_\alpha, \qquad \mathbf{A}_\alpha = \mathbf{A}'_\alpha + \mathrm{i}\mathbf{A}''_\alpha. \tag{15}$$

The vectors $\mathbf{A}_\alpha$ are assumed normalized in accordance with the rule

$$|\mathbf{A}_\alpha| = 1, \qquad \mathbf{A}'_\alpha\mathbf{A}''_\alpha = 0. \tag{16}$$

These vectors are mutually orthogonal in nondegenerate directions: $\mathbf{A}_\alpha\mathbf{A}_\beta = 0$ ($\alpha \neq \beta$).

We consider solutions for the universal wave, Eqn (14), with the propagation directions $\mathbf{m}$ lying in a close vicinity of the conical degeneracy direction $\mathbf{m}_0$:

$$\mathbf{m} = \mathbf{m}_0 + \Delta\mathbf{m}, \qquad |\mathbf{m}| = |\mathbf{m}_0| = 1, \qquad |\Delta\mathbf{m}| \ll 1. \tag{17}$$

In a crystal without absorption, the phase velocities of two isonormal waves along the degenerate direction $\mathbf{m}_0$ coincide, $v_1 = v_2 = v_0$, and their polarization is arbitrary in the D-plane, called the degeneracy plane. When absorption is included, the velocity changes $\Delta v_{1,2}$ and polarization vectors $\mathbf{A}_{1,2}$ of isonormal waves near the direction $\mathbf{m}_0$ are given by

$$\Delta v_{1,2} = \mathbf{s}^0\Delta\mathbf{m} - \mathrm{i}s'' \mp R, \qquad \mathbf{A}_{1,2} \parallel -(\mathbf{q}\Delta\mathbf{m} - \mathrm{i}q'')\mathbf{A}_{01} + (\mathbf{p}\Delta\mathbf{m} - \mathrm{i}p'' \pm R)\mathbf{A}_{02}, \qquad R = \sqrt{(\mathbf{p}\Delta\mathbf{m} - \mathrm{i}p'')^2 + (\mathbf{q}\Delta\mathbf{m} - \mathrm{i}q'')^2}. \tag{18}$$

The vectors $\mathbf{s}^0$, $\mathbf{p}$, and $\mathbf{q}$ and the scalar absorption parameters p'', q'', and s'' introduced in (18) are determined by convolutions of the vectors $\mathbf{A}_{01}$, $\mathbf{A}_{02}$, and $\mathbf{m}_0$ with tensors $\hat{\Lambda}'$ and $\hat{\Lambda}''$:

$$\left.\begin{matrix} \mathbf{s}^0 \\ \mathbf{p} \end{matrix}\right\} = \frac{1}{2v_0}(\mathbf{A}_{01}\hat{\Lambda}'\mathbf{A}_{01} \pm \mathbf{A}_{02}\hat{\Lambda}'\mathbf{A}_{02})\mathbf{m}_0, \qquad \mathbf{q} = \frac{1}{2v_0}(\mathbf{A}_{01}\hat{\Lambda}'\mathbf{A}_{02} + \mathbf{A}_{02}\hat{\Lambda}'\mathbf{A}_{01})\mathbf{m}_0, \tag{19}$$

$$\left.\begin{matrix} s'' \\ p'' \end{matrix}\right\} = \frac{Q''_{11} \pm Q''_{22}}{4v_0}, \qquad q'' = \frac{Q''_{12}}{2v_0}, \qquad Q''_{ij} = \mathbf{A}_{0i}\hat{Q}''_0\mathbf{A}_{0j}, \quad \hat{Q}''_0 = \hat{Q}''(\mathbf{m}_0). \tag{20}$$

Here, the vectors $\mathbf{s}^0$, $\mathbf{p}$, and $\mathbf{q}$ have the properties

$$\mathbf{s}^0\mathbf{m}_0 = v_0, \qquad \mathbf{pm}_0 = \mathbf{qm}_0 = 0. \tag{21}$$

The smallness of the deviation $\Delta\mathbf{m} = \mathbf{m} - \mathbf{m}_0$ of the unit wave normal $\mathbf{m}$ from the direction $\mathbf{m}_0$ of the initial degeneracy in (18) is determined by the possibility of neglecting the components of vectors $\mathbf{A}_{1,2}$ along $\mathbf{A}_{03}$ of the order $(\Delta\mathbf{m})^2$ in (18).

For weak absorption, the components of complex velocities and wave numbers are related as

$$k'_\alpha = \frac{\omega}{v_0}\left(1 - \frac{\Delta v'_\alpha}{v_0}\right), \qquad k''_\alpha = v''_\alpha\left(\frac{\omega}{v_0^2}\right). \tag{22}$$

We can see from (18) and (22) that the requirement of the decay of isonormal waves during propagation, $k''_\alpha > 0$, determines the stability criterion $s''_{ac} > |\mathrm{Im}\, R|$.

In isotropic media, material tensors $\hat{\Lambda}'$ and $\hat{\Lambda}''$ in (13) are such that their convolutions with basis vectors $\mathbf{A}_{01}$ and $\mathbf{A}_{02}$, the quantities $\mathbf{p}$, $\mathbf{q}$, p'', and q'' in (19) and (20), vanish (but $\mathbf{s}^0$ and s'' do not in this case). Therefore, the effects considered here are entirely caused by anisotropy and are specific exclusively to crystals.

Optical second-rank tensors $\hat{\varepsilon}^{-1}$ and $\hat{\delta}$ are simpler than acoustic fourth-rank tensors $\hat{c}$ and $\hat{\eta}$. Because of this, the vectors $\mathbf{s}^0_{op}$, $\mathbf{p}_{op}$, $\mathbf{q}_{op}$ and the scalars s''_{op}, p''_{op}, q''_{op} can be explicitly calculated as compact functions of the eigenvalues of $\hat{\varepsilon}^{-1}$ and components of $\hat{\delta}$ in basis (11):

$$\mathbf{s}^0_{op} = (-\lambda\mathbf{A}_{01} + \mathbf{A}_{03})v_0\,, \qquad \mathbf{s}^0_{op}\mathbf{m}_0 = v_0\,,$$

$$\mathbf{p}_{op} = \lambda v_0\mathbf{A}_{01}\,, \qquad \mathbf{q}_{op} = \lambda v_0\mathbf{A}_{02}\,, \qquad \mathbf{p}_{op}\mathbf{q}_{op} = 0\,, \tag{23}$$

$$\lambda = \frac{1}{2}\sqrt{\frac{(\varepsilon_3-\varepsilon_2)(\varepsilon_2-\varepsilon_1)}{\varepsilon_1\varepsilon_3}}\,, \qquad v_0 = \frac{c}{\sqrt{\varepsilon_2}}\,,$$

$$\left.\begin{matrix} s''_{op} \\ p''_{op} \end{matrix}\right\} = \frac{v_0\varepsilon_2}{4}(\delta_{22} \pm \delta_{11})\,, \qquad q''_{op} = -\frac{v_0\varepsilon_2}{2}\,\delta_{12}\,. \tag{24}$$

An important remark must be made here. A transparent biaxial crystal has a rhombic symmetry with respect to its optical properties, even being triclinic with respect to other properties, for example, acoustic ones. This is explained by the fact that the permittivity tensor $\hat{\varepsilon}$, as any second-rank tensor, has the symmetry of its characteristic ellipsoid: it has three mutually orthogonal symmetry planes coinciding with the coordinate planes of the $\{X, Y, Z\}$ system (Fig. 2a). The inclusion of absorption adds another second-rank tensor $\hat{\delta}$, which, of course, has the same symmetry elements. But these tensors are diagonalized in different coordinate systems in a triclinic crystal, i.e., their symmetry planes do not coincide in general. In the particular case of monoclinic crystals, both tensors $\hat{\varepsilon}$ and $\hat{\delta}$ share one symmetry plane.

We have thus arrived at a unified mathematical formalism that can be used to describe both elastic and electromagnetic fields in triclinic crystals. General solutions (18)–(20) determining the key characteristics of the waves, with the correspondence relations (12) and (13) taken into account, describe both the acoustics and the optics of absorptive crystals. Of course, the main topological features of the wave fields of the two types are then similar near degeneracies.

However, for the abovementioned reasons, geometrical and topological features in optics are often more symmetric than in acoustics. For example, in acoustics, the vectors $\mathbf{p}$ and $\mathbf{q}$ in (19) are not orthogonal and have different lengths in general, whereas the corresponding vectors (23) in optics are orthogonal and have the same length. We can see from Fig. 1 that the vector $\mathbf{A}_{03}$ in acoustics generally deviates from the direction $\mathbf{m}_0$, whereas these vectors coincide in optics (Fig. 2b), $\mathbf{A}_{03} = \mathbf{m}_0$. Moreover, polarization topological singularities can appear in acoustics, which are impossible in optics.

3. Topological features of wave surfaces

3.1 Splitting of acoustic and optical axes

The inclusion of absorption leads to the splitting of the initial conical degeneracy along $\mathbf{m}_0$ into two new degeneracies, $\mathbf{m}_0^{\pm} \equiv \mathbf{m}_0 \pm \Delta\mathbf{m}_0$. Singular optical and acoustic axes appear, the complex velocities of isonormal waves propagating along them being coincident: $v_1 = v_2$. The directions of singular axes are determined from the general condition $R(\Delta\mathbf{m}) = 0$, where the radical R is defined in (18). This gives the splitting vector $\Delta\mathbf{m}_0$, which is the same for acoustics and optics:

$$\Delta\mathbf{m}_0 = \frac{r}{g}\,\mathbf{m}_0 \times \mathbf{M}\,. \tag{25}$$

Here, the notation

$$\mathbf{M} = \mathbf{p}\sin\alpha + \mathbf{q}\cos\alpha\,,$$

$$\sin\alpha = \frac{p''}{r}\,, \qquad \cos\alpha = \frac{q''}{r}\,, \tag{26}$$

$$r = \sqrt{p''^2 + q''^2}\,, \qquad g = \mathbf{m}_0(\mathbf{p}\times\mathbf{q})$$

is introduced. It follows from (25) and (26) that

$$\Delta\mathbf{m}_0\mathbf{p} = -q''\,, \qquad \Delta\mathbf{m}_0\mathbf{q} = p''\,. \tag{27}$$

The splitting angle $\Delta\Psi \approx 2|\Delta\mathbf{m}_0|$ of the axes is proportional to absorption, the factor r in (26).

General expressions (25) and (26) can now easily be specified in optics:

$$\mathbf{M} = \lambda v_0\boldsymbol{\tau}_\perp\,, \qquad \mathbf{m}_0 \times \mathbf{M} = \lambda v_0\boldsymbol{\tau}_\parallel\,,$$

$$r = \frac{v_0\varepsilon_2}{4}\sqrt{(\delta_{11}-\delta_{22})^2 + 4\delta_{12}^2}\,, \qquad g = \lambda^2 v_0^2\,. \tag{28}$$

Here, the unit mutually orthogonal vectors $\boldsymbol{\tau}_\perp$ and $\boldsymbol{\tau}_\parallel$ are introduced as (Fig. 3a)

$$\boldsymbol{\tau}_\perp = \mathbf{A}_{01}\sin\alpha + \mathbf{A}_{02}\cos\alpha\,,$$

$$\boldsymbol{\tau}_\parallel = -\mathbf{A}_{01}\cos\alpha + \mathbf{A}_{02}\sin\alpha\,, \tag{29}$$

$$\boldsymbol{\tau}_\perp \times \boldsymbol{\tau}_\parallel = \mathbf{m}_0\,.$$

The relation between unit vectors $\{\mathbf{A}_{01}, \mathbf{A}_{02}\}$ and $\{\boldsymbol{\tau}_\perp, \boldsymbol{\tau}_\parallel\}$ on which the two coordinate systems, $\{x, y\}$ and $\{x', y'\}$ are respectively constructed is shown in Fig. 3a.

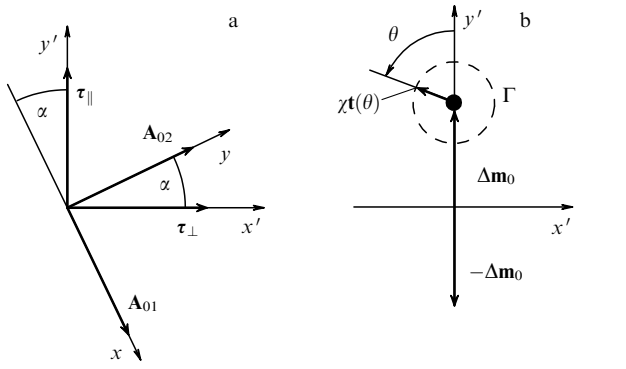

Figure 3. (a) Mutual orientation of two pairs of unit vectors $\{\mathbf{A}_{01}, \mathbf{A}_{02}\}$ and $\{\boldsymbol{\tau}_\perp, \boldsymbol{\tau}_\parallel\}$ on which coordinate systems $\{x, y\}$ and $\{x', y'\}$ are constructed. (b) Vectors $\Delta\mathbf{m}_0$ and $\chi\mathbf{t}$ in the $\{x', y'\}$ system on the contour Γ.

Now, expression (25) for $\Delta\mathbf{m}_0$ takes the form (Fig. 3b)

$$\Delta\mathbf{m}_0 = \boldsymbol{\tau}_\parallel \frac{\varepsilon_2}{4\lambda}\sqrt{(\delta_{11}-\delta_{22})^2+4\delta_{12}^2}\,. \tag{30}$$

As can be seen from Fig. 3 and expressions (25) and (30), both in acoustics and in optics, the splitting vector $\Delta\mathbf{m}_0$ is in a general position in the plane perpendicular to the vector $\mathbf{m}_0$, which is natural for triclinic crystals. The concrete orientation (the angle α) of $\Delta\mathbf{m}_0$ in this plane is determined by the relation between absorption parameters p'' and q'', as follows from (26).

It follows from (30) that the splitting of optical axes is determined by the ratio of the anisotropy parameter of the absorption tensor $\hat{\delta}$ in (5) to the dielectric anisotropy parameter λ in (23). In optics, therefore, the splitting can be increased not only by increasing absorption but also by selecting crystals for which $\lambda \ll 1$ (see Section 6).

The foregoing applies to crystals with an arbitrary anisotropy. The inclusion of symmetry elements can be significant. For example, it can be shown [12] that tangential acoustic axes [17] are not split along symmetry axes 6 and 4 because $\mathbf{p}_{ac} = \mathbf{q}_{ac} = p''_{ac} = q''_{ac} = 0$ along these axes and $\Delta\mathbf{m}_0 = 0$ according to (25). Along symmetry axis 3, a conical degeneracy is realized [17], but absorption does not likewise split it [12] because, in this case, $p''_{ac} = q''_{ac} = r = 0$ and therefore $\Delta\mathbf{m}_0 = 0$. In the optics of uniaxial crystals, all the symmetry axes mentioned above correspond to tangential degeneracies and do not split in the presence of absorption for the same reasons. On the other hand, if an absorptive crystal has a symmetry axis S and the initial degeneracy direction $\mathbf{m}_0$ belongs to this plane, splitting occurs in both acoustics and optics, its description being simplified. In this case, $q'' = 0$, $\alpha = \pi/2$, the vector $\mathbf{q}$ is orthogonal to the plane S, the vector $\mathbf{p}$ belongs to S, and $\Delta\mathbf{m}_0 \parallel \mathbf{q}$. Here, $\delta_{12} = 0$ and expressions (28) and (30) are simplified.

3.2 Self-intersection lines of the phase velocity surface

We consider the wave normal $\mathbf{m}_\gamma$ specified by the relation

$$\mathbf{m}_\gamma = \mathbf{m}_0 + \gamma\Delta\mathbf{m}_0\,. \tag{31}$$

As the value of γ ranges the interval $-1 \leqslant \gamma \leqslant 1$, the end of the vector $\mathbf{m}_\gamma$ on the unit sphere traces a line connecting the directions of singular axes $\mathbf{m}_0^-$ (for $\gamma = -1$) and $\mathbf{m}_0^+$ (for $\gamma = 1$). It is easy to verify that the radical R in (18) is purely imaginary on this line, and therefore these lines are equal-velocity lines in both acoustics and optics: $v'_1(\mathbf{m}_\gamma) = v'_2(\mathbf{m}_\gamma)$. Only the difference in the intensity of absorption of isonormal waves is preserved. Due to absorption, intersection lines appear instead of conical point contacts between the velocity surface sheets, which means that the topology of the surface changes (Fig. 4).

We consider the features of the local geometry of such a surface near degeneracies in the simpler optical case. Let the wave normal $\mathbf{m}$ go around the singular axis $\mathbf{m}_0^+ = \mathbf{c}_I + \Delta\mathbf{m}_0$ along a small circular contour Γ with a radius χ (Fig. 3b):

$$\begin{aligned}&\mathbf{m} = \mathbf{m}_0^+ + \chi\mathbf{t}(\theta)\,, \qquad \mathbf{t}(\theta) = \boldsymbol{\tau}_\parallel\cos\theta - \boldsymbol{\tau}_\perp\sin\theta\,,\\ &0 < \chi \ll |\Delta\mathbf{m}_0|\,, \qquad 0 \leqslant \theta < 2\pi\,.\end{aligned} \tag{32}$$

The dependence of the complex velocities $v_{1,2}$ in (18) on the parameters χ and θ on this contour has the form

$$v_{1,2} = v_0^+ \mp R(\chi,\theta)\,, \tag{33}$$

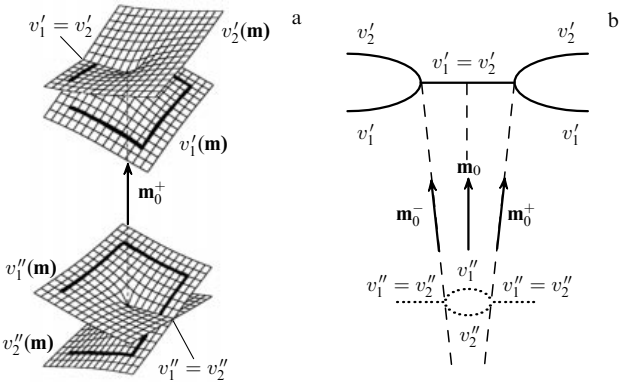

Figure 4. Geometry of sheets of the velocity surface $v'_{1,2}(\mathbf{m})$ and the absorption surface $v''_{1,2}(\mathbf{m})$: (a) in a three-dimensional scheme near the singular axis $\mathbf{m}_0^+$, (b) section of surfaces by the plane of split axes $\mathbf{m}_0^+$ and $\mathbf{m}_0^-$.

where

$$v_0^+ = v_0 + \mathbf{s}^0_{op}\Delta\mathbf{m}_0 - \mathrm{i}s''_{op} \tag{34}$$

is the phase velocity along the singular $\mathbf{m}_0^+$ axis and R is the radical in (18), which has the form

$$R(\chi,\theta) \approx \sqrt{2\chi\lambda r v_0}\,\exp\frac{\mathrm{i}\theta}{2} \tag{35}$$

up to terms $\sim \chi^{3/2}$. Hence, the velocity surface $v'_{1,2}(\chi,\theta)$ in the region of parameters χ and θ under study is given by

$$\begin{aligned}&v'_{1,2}(\chi,\theta) \approx v_0 + \mathbf{s}^0_{op}\Delta\mathbf{m}_0 \mp \sqrt{2\chi\lambda r v_0}\,\cos\frac{\theta}{2}\,,\\ &-\pi \leqslant \theta \leqslant \pi\,.\end{aligned} \tag{36}$$

For $\theta = \pm\pi$, we have $v'_1 = v'_2 = v'^+_0$ in this approximation, which means that the wave normal is on the equal-velocity line, which can be treated as a wedge edge (Fig. 4a). In each section $\theta = \mathrm{const} \neq \pm\pi$, the derivative of $v'_{1,2}(\chi,\theta)$ with respect to χ,

$$\frac{\partial v'_{1,2}}{\partial\chi} = \mp\sqrt{\frac{\lambda r v_0}{\chi}}\,\cos\frac{\theta}{2}\,, \tag{37}$$

tends to infinity as $\chi \to 0$. Such a singular dependence of this function at the wedge edge corresponds to a cusp of the velocity surface and a flat fan of normals $\mathbf{n}(\theta)$ to this surface on the contour under study for $\chi \to 0$. The local geometry described by expressions (36) and (37) is illustrated in Figs 4 and 5a. Figure 5b illustrates another feature of the contact

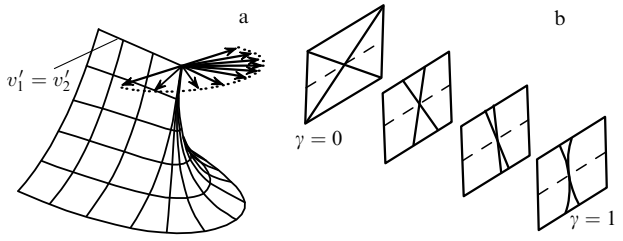

Figure 5. (a) Cusp configurations on the refraction surface near one of the ends of the wedge edge. (b) Change in the geometry of the sheet contact on the line γ in a series of sections of the same surface by planes perpendicular to the edge.

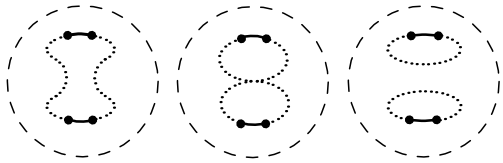

Figure 6. Scheme of the topological reconstruction of equal-velocity lines (solid lines) and equal-absorption lines (dotted lines) with varying the dielectric anisotropy parameters. Stereographic projections are presented.

geometry under study: at a very short distance from the wedge middle ($\gamma = 0$) to the singular axis ($\gamma = 1$), the section of the surface perpendicular to the wedge edge is transformed from an obtuse angle to an infinitely sharp joint of two touching parabolas.

3.3 Self-intersection lines of the absorption surface

The inclusion of dissipation in both acoustics and optics leads to the appearance of absorption surfaces, which were initially absent. They characterize the decay of waves depending on the propagation direction **m**. Such a surface is a locus of the ends of radius vectors $v''_\alpha \mathbf{m}$ as the vector **m** ranges the unit sphere $\mathbf{m}^2 = 1$. In crystal optics, these are two-sheet surfaces, $\alpha = 1, 2$, while in acoustics they are three-sheet surfaces, $\alpha = 1, 2, 3$. In acoustics, however, we are also interested only in two sheets ($\alpha = 1, 2$) between which intersection lines appear.

In optics, according to (33)–(35), the dependence of the absorption intensity $v''_\alpha(\chi, \theta)$ on the position of the observation point on the contour Γ (Fig. 3b) surrounding the $\mathbf{m}_0^+$ axis is similar to (36):

$$v''_{1,2}(\chi, \theta) \approx s''_{\mathrm{op}} \pm \sqrt{2\chi\lambda r v_0}\, \sin\frac{\theta}{2}\,, \qquad 0 \leqslant \theta < 2\pi\,. \tag{38}$$

We can see from (38) that for $\theta = 0$, the wave normal falls on the equal-absorption line, $v''_1(\chi, 0) = v''_2(\chi, 0) \approx s''_{\mathrm{op}}$. The radical R is then real and the difference between the velocities $v'_{1,2}$ of isonormal waves is preserved. We can see from Fig. 4 that such lines on the sphere $\mathbf{m}^2 = 1$ appear as a continuation of the wedge edge of the velocity surface on both of its ends. Being a continuation of each other on the direction sphere, the equal-velocity and equal-absorption lines share points corresponding to singular axes. Of course, due to weak absorption, the angular extension of the equal-velocity lines is much smaller than that of equal-absorption lines.

The configurations of lines of these two types in the optics of absorptive crystals were considered in [18]. The analysis was performed for weak dielectric anisotropy at which sheets and velocity surfaces, as well as absorption surfaces, are close to each other. The curves under study are closed and consist of alternating fragments corresponding to equal velocities and equal absorptions. As the tensors $\hat{\varepsilon}$ and $\hat{\delta}$ are varied, drastic changes in topology can occur [19]: for example, a closed curve can split into two closed curves, as shown in Fig. 6.

We note, incidentally, that the nontrivial aspects of the influence of absorption on the properties of optical and acoustic waves in crystalline materials, including topological effects, are currently attracting increasing attention (see, e.g., [20, 21]), in particular, due to their diverse applications in acoustoelectronics and acoustooptics.

4. Topological features in polarization fields

4.1 Distribution of polarization ellipses in the vicinity of split axes

In this section, we consider the features of the distribution of complex vector polarization fields in the vicinity of a pair of split axes.

After normalization (16), the vectors $\mathbf{A}_{1,2}(\mathbf{m})$ in (18) take the form

$$\mathbf{A}_{1,2} = \frac{\mathbf{A}_{01} + (f \pm Q)\mathbf{A}_{02}}{\sqrt{1 + |f \pm Q|^2}}\, \exp\left(-\mathrm{i}\Theta_\pm\right), \tag{39}$$

where

$$f = -\frac{\mathbf{p}\Delta\mathbf{m} - \mathrm{i}p''}{\mathbf{q}\Delta\mathbf{m} - \mathrm{i}q''}\,, \qquad Q = \sqrt{1 + f^2}\,, \qquad \Theta_\pm = \frac{1}{2}\arg\left[Q(Q \pm f)\right]. \tag{40}$$

Complex vectors $\mathbf{A}_\alpha \equiv \mathbf{A}'_\alpha + \mathrm{i}\mathbf{A}''_\alpha$ ($\alpha = 1, 2$) describe two conical polarization ellipses with half-axes whose length and orientation are specified by mutually orthogonal radius vectors $\mathbf{A}'_\alpha$ and $\mathbf{A}''_\alpha$. The ellipticity ϵ of isonormal waves is defined as the ratio of the minor and major semiaxes A''_α and A'_α. According to [6],

$$\epsilon = \frac{A''_{1,2}}{A'_{1,2}} = \sqrt{\frac{1 - \kappa}{1 + \kappa}}\,, \tag{41}$$

where, in accordance with (39), we should set

$$\kappa = |\mathbf{A}^2_{1,2}| = \frac{2|Q|F_{1,2}}{1 + F^2_{1,2}}\,, \tag{42}$$

$$F_{1,2} = |Q \pm f|\,. \tag{43}$$

The ellipticities of two isonormal waves are equal,

$$\frac{A''_1}{A'_1} = \frac{A''_2}{A'_2} \equiv \epsilon\,, \tag{44}$$

which follows from the orthogonality of the vectors $\mathbf{A}_1$ and $\mathbf{A}_2$ and is also seen from (42). Taking (40) and (43) into account, we see that the parameters F_1 and F_2 are mutually inverse:

$$F_1 F_2 = |Q^2 - f^2| = 1\,. \tag{45}$$

This allows us to bring expression (42) to the form

$$|\mathbf{A}^2_1| = \frac{2|Q|F_1}{1 + F_1/F_2} = \frac{2|Q|}{F_1 + F_2} = |\mathbf{A}^2_2| \equiv \kappa\,. \tag{46}$$

Accordingly, expression (41) is also independent of the branch number.

We consider the distribution of vector fields $\mathbf{A}_{1,2}(\mathbf{m})$ on the unit sphere $\mathbf{m}^2 = 1$ beginning from the line γ in (31) of the self-intersection edge of wave surfaces, which passes through the degeneracy points $\mathbf{m}_0^\pm = \mathbf{m}_0 \pm \Delta\mathbf{m}_0$. We recall that the γ axis has its origin at the edger center corresponding to the vector $\mathbf{m}_0$ and its scale is measured by the length of $\Delta\mathbf{m}_0$, Eqn (25):

$$\Delta\mathbf{m} = \gamma\Delta\mathbf{m}_0\,. \tag{47}$$

The positions of singular axes $\mathbf{m}_0^{\pm}$ correspond to the values $\gamma = \pm 1$. Between the axes in the region $|\gamma| < 1$, we are at the self-intersection edge of the slowness surface, and for $|\gamma| > 1$, we pass to self-intersection lines of the absorption surface. With the initial assumption $|\Delta\mathbf{m}| \ll 1$ of our formalism, it is obvious that the region of admissible values of $|\gamma| = |\Delta\mathbf{m}|/|\Delta\mathbf{m}_0|$ is bounded above, but it can be broad enough for small splittings $|\Delta\mathbf{m}_0|$, which is almost always the case due to weak absorption.

Substituting (47) in (40) and taking (25)–(27) into account, we obtain

$$f = \frac{\gamma\cos\alpha + \mathrm{i}\sin\alpha}{\gamma\sin\alpha - \mathrm{i}\cos\alpha}\,, \qquad Q = \frac{\sqrt{\gamma^2 - 1}}{\gamma\sin\alpha - \mathrm{i}\cos\alpha}\,. \tag{48}$$

It follows from (48) and (40) that the parameters f, Q, and $\Theta_{\pm}$ at the points $\gamma = \pm 1$ corresponding to singular axes take the values

$$f = \pm\mathrm{i}\,, \quad Q = 0\,, \quad \Theta_{\pm} = 0\,. \tag{49}$$

In this case, expression (39) gives

$$\mathbf{A}_1(\mathbf{m}_0^{\pm}) = \mathbf{A}_2(\mathbf{m}_0^{\pm}) = \frac{\mathbf{A}_{01} \pm \mathrm{i}\mathbf{A}_{02}}{\sqrt{2}}\,, \tag{50}$$

which means that degenerate waves along singular axes $\mathbf{m} = \mathbf{m}_0^{\pm}$ are circularly polarized. The same conclusion follows from (41) and (42): for $Q = 0$, we obtain $\kappa = 0$ and $\epsilon = 1$.

At the point $\gamma = 0$ corresponding to the direction $\mathbf{m}_0$, we have

$$f = -\tan\alpha\,, \quad Q = -\sec\alpha\,, \quad \Theta_{\pm} = 0 \tag{51}$$

instead of (49). In this case, the parameters f and Q are real, and therefore polarization is linear:

$$\begin{aligned} \mathbf{A}_1 &= \mathbf{A}_{01}\sin\left(\frac{\pi}{4} - \frac{\alpha}{2}\right) - \mathbf{A}_{02}\cos\left(\frac{\pi}{4} - \frac{\alpha}{2}\right), \\ \mathbf{A}_2 &= \mathbf{A}_{01}\cos\left(\frac{\pi}{4} - \frac{\alpha}{2}\right) + \mathbf{A}_{02}\sin\left(\frac{\pi}{4} - \frac{\alpha}{2}\right). \end{aligned} \tag{52}$$

It is important that the discovered linear polarization is preserved on the entire line intersecting the wedge edge at its center $\mathbf{m} = \mathbf{m}_0$. Obviously, the orientation of this line corresponds to the direction of $\Delta\mathbf{m}$ along which the real value of the parameter f in (40) is preserved. Indeed, the parameter Q in this case is also real and κ in (46) is equal to unity, while ellipticity (41) vanishes. The requirement $\mathrm{Im}\, f = 0$ applied to expression (40) is equivalent to the equation

$$\Delta\mathbf{m}\,\mathbf{N} = 0\,, \qquad \mathbf{N} = -\mathbf{p}\cos\alpha + \mathbf{q}\sin\alpha\,. \tag{53}$$

In other words, the zero-ellipticity line on the sphere $\mathbf{m}^2 = 1$ must be directed along the vector $\mathbf{m}_0 \times \mathbf{N}$. According to (25) and (26), the wedge edge is parallel to the vector $\mathbf{m}_0 \times \mathbf{M}$. Hence, the wedge-edge line and zero-ellipticity line belong to a plane perpendicular to $\mathbf{m}_0$, and the angle between them is equal to that between the vectors $\mathbf{N}$ and $\mathbf{M}$, which are not orthogonal to each other in general (Fig. 7).

In optics, the direction of the line η of solutions for zero-ellipticity lines is orthogonal to the wedge edge because we then have $\mathbf{m}_0 \times \mathbf{N} \parallel \boldsymbol{\tau}_{\perp}$, $\mathbf{m}_0 \times \mathbf{M} \parallel \boldsymbol{\tau}_{\parallel}$, and $\boldsymbol{\tau}_{\perp} \perp \boldsymbol{\tau}_{\parallel}$ (Fig. 3a). In

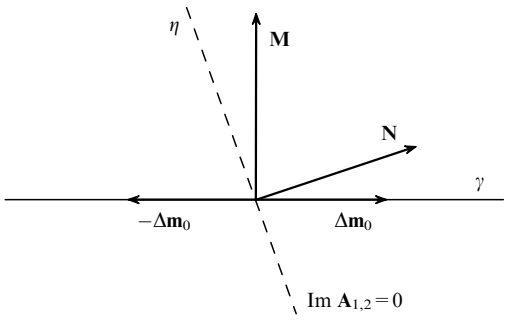

Figure 7. Zero-ellipticity line (dashed straight line $\eta \perp \mathbf{N}$) and the self-intersection line (solid straight line $\gamma \perp \mathbf{M}$) in a plane orthogonal to the vector $\mathbf{m}_0$.

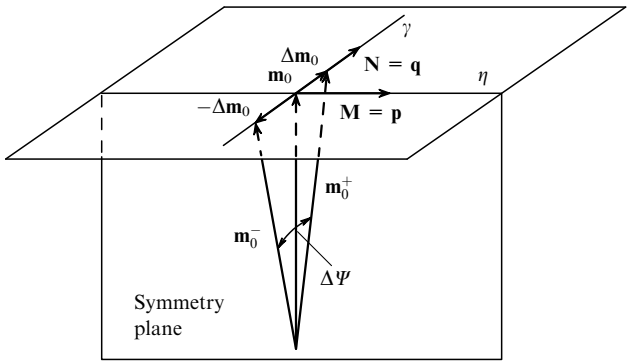

Figure 8. Geometry of the $\mathbf{m}_0 \to \mathbf{m}_0^{\pm}$ splitting of the acoustic (optic) axis from the symmetry plane of a crystal when taking absorption into account.

acoustics, such orthogonality appears when the initial degeneracy direction $\mathbf{m}_0$ belongs to the symmetry plane m of the crystal, because in this case, $q'' = 0$, $\alpha = \pi/2$, $\mathbf{M} = \mathbf{p} \subset m$, and $\mathbf{N} = \mathbf{q} \perp m$ (Fig. 8). But as we see in what follows, the parameter f remains complex for $q'' = 0$, while the linear polarization along the direction $\Delta\mathbf{m} \parallel \mathbf{M}$ is provided by the symmetry.

Below, we consider the polarization distribution just in this case, convenient for the analysis, in the geometry shown in Fig. 8. As mentioned above, the vector $\mathbf{q} \parallel \mathbf{A}_{02}$, which is orthogonal to the m plane, specifies the splitting direction $\Delta\mathbf{m}_0$ of the axes, while the vectors $\mathbf{A}_{01}$ and $\mathbf{A}_{03}$ are parallel to the m plane; the vector $\mathbf{A}_{01}$ is necessarily collinear to the vector $\mathbf{p} \subset m$ only in optics, Eqn (23), but not in acoustics in general.

Because the lines $\gamma \parallel \Delta\mathbf{m}_0 \parallel \mathbf{q} = \mathbf{N}$ and $\eta \parallel \mathbf{p} = \mathbf{M}$ are orthogonal (see Fig. 8), it is convenient to use them as an auxiliary coordinate system by decomposing the vector $\Delta\mathbf{m}$ as

$$\Delta\mathbf{m} = \gamma\Delta\mathbf{m}_0 + \eta\,\frac{p''}{p^2}\,\mathbf{p}\,. \tag{54}$$

The scale along the γ axis is the same ($|\Delta\mathbf{m}_0|$), while the scale along the η axis is different (p''/p). The latter scale differs from the former by a factor of the order of unity:

$$\frac{p''}{p} = |\Delta\mathbf{m}_0|\,\frac{q}{p}\,. \tag{55}$$

Such a difference makes expressions derived below more compact. However, these scales are the same in optics, because $p_{\mathrm{op}} = q_{\mathrm{op}}$ according to (23).

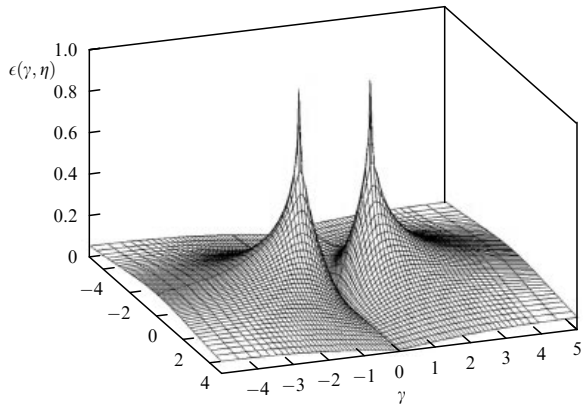

Figure 9. Two peaks of the ellipticity surface $\epsilon(\gamma,\eta)$ in the vicinity of split axes.

Substituting (54) in (40), we obtain

$$f=\frac{1}{\gamma}(\mathrm{i}-\eta)\,,\quad Q=\frac{1}{\gamma}\sqrt{w-2\mathrm{i}\eta}\,,\quad w=\gamma^2+\eta^2-1\,. \tag{56}$$

With these expressions, after a number of transformations of (42), we find

$$\kappa=\sqrt{\frac{2}{1+G(\gamma,\eta)}}\,, \tag{57}$$

where

$$G=\frac{w+2}{\sqrt{w^2+4\eta^2}}\,. \tag{58}$$

Combining expressions (57) and (58) with (41), we readily find the total ellipticity distribution $\epsilon(\gamma,\eta)$ in the vicinity of the split degeneracies under study. The result is presented in the form of the three-dimensional plot in Fig. 9.

We consider cross sections of this surface. We begin with the distribution of the polarization ellipticity on the γ axis. Setting $\eta=0$ in (57) and (58), we obtain from (41) that

$$\epsilon=\begin{cases}\left(\dfrac{1-\sqrt{1-\gamma^2}}{1+\sqrt{1-\gamma^2}}\right)^{1/2}, & |\gamma|\leqslant 1\,,\\[2ex] \left(\dfrac{1-\sqrt{1-1/\gamma^2}}{1+\sqrt{1-1/\gamma^2}}\right)^{1/2}, & |\gamma|\geqslant 1\,,\end{cases}\approx\begin{cases}\dfrac{|\gamma|}{2}\,, & |\gamma|\ll 1\,,\\[2ex] \dfrac{1}{2|\gamma|}\,, & |\gamma|\gg 1\,.\end{cases} \tag{59}$$

It follows from Fig. 10a, where the ellipticity distribution is shown, that polarization is circular at the reference points $\gamma=\pm 1$ corresponding to singular axes ($\Delta\mathbf{m}=\pm\Delta\mathbf{m}_0$), as before, and is still linear at the point $\gamma=0$.

We note that after the substitution

$$\gamma=\begin{cases}\sin\xi\,, & |\gamma|\leqslant 1\,,\quad -\dfrac{\pi}{2}\leqslant\xi\leqslant\dfrac{\pi}{2}\,,\\[2ex] \operatorname{cosec}\zeta\,, & |\gamma|\geqslant 1\,,\quad -\dfrac{\pi}{2}\leqslant\zeta\leqslant\dfrac{\pi}{2}\,,\end{cases} \tag{60}$$

expressions (59) become remarkably compact:

$$\epsilon=\begin{cases}\left|\tan\dfrac{\xi}{2}\right|, & |\gamma|\leqslant 1\,,\\[2ex] \left|\tan\dfrac{\zeta}{2}\right|, & |\gamma|\geqslant 1\,.\end{cases} \tag{61}$$

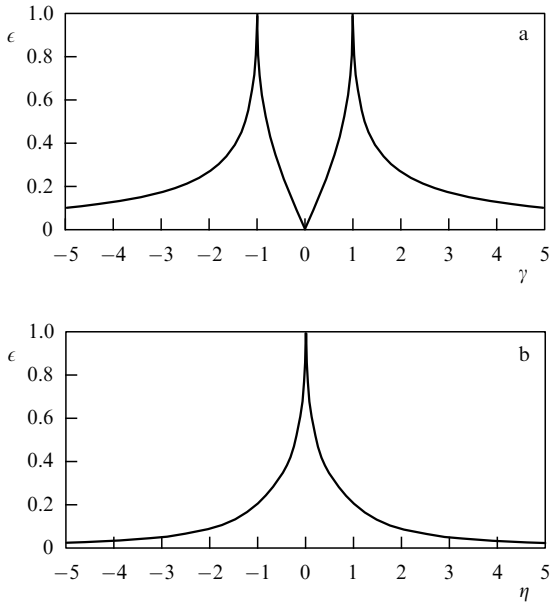

Figure 10. Cross sections of the surface $\epsilon(\gamma,\eta)$ shown in Fig. 9, by vertical planes: (a) $\eta=0$, (b) $\gamma=\pm 1$.

Similarly, polarization vectors (39) in the cross section $\eta=0$ under study become

$$\left.\begin{aligned}\mathbf{A}_1&=\mathbf{A}_{02}\cos\frac{\xi}{2}-\mathrm{i}\mathbf{A}_{01}\sin\frac{\xi}{2}\,,\\ \mathbf{A}_2&=\mathbf{A}_{01}\cos\frac{\xi}{2}+\mathrm{i}\mathbf{A}_{02}\sin\frac{\xi}{2}\,,\end{aligned}\right\}\quad |\gamma|<1\,, \tag{62}$$

$$\mathbf{A}_{1,2}=\frac{1}{\sqrt{2}}\left[(\mathbf{A}_{01}\pm\mathbf{A}_{02})\cos\frac{\zeta}{2}+\mathrm{i}(\mathbf{A}_{02}\mp\mathbf{A}_{01})\sin\frac{\zeta}{2}\right],\quad |\gamma|>1\,. \tag{63}$$

The second cross section of interest to us is the vertical plane $\gamma=0$ passing through the η axis. As noted when discussing Figs 7 and 8, linear polarization should occur on the η axis, which is partially seen in Figs 9 and 10a (in Fig. 10a, the zero-ellipticity line is projected to the point $\gamma=0$). We demonstrate this analytically. Substituting $w=\eta^2-1$ in (59), we obtain $G=1$. It then follows from (58) that $\kappa=1$. Therefore, according to (41), the ellipticity is zero, $\epsilon=0$, i.e., the polarization is linear.

Also of interest are two other vertical sections passing through the degeneracy points $\gamma=\pm 1$, which are also orthogonal to the γ axis. These sections have the same symmetry and are of course identical. They are analytically described by the same expression (41) after the substitution of (57) and (58) in it, with the relation $w=\eta^2$ assumed. Here, we present only approximate dependences in the limit cases $|\eta|\ll 1$ and $|\eta|\gg 1$:

$$\epsilon\approx\begin{cases}1-\sqrt{2|\eta|}\,, & |\eta|\ll 1\,,\\[2ex] \dfrac{1}{2\eta^2}\,, & |\eta|\gg 1\,.\end{cases} \tag{64}$$

The shape of sections for $\gamma=\pm 1$ is shown in Fig. 10b. We can see from expressions (59), (64) and Figs 9 and 10 that the cusps of the ellipticity profile at the points $\gamma=\pm 1$ and $\eta=0$ have vertical tangents in the vertical sections under study (and in any others) passing through these points.

4.2 Polarization singularities around degeneracy directions
As shown in Section 4.1, if the wave normal $\mathbf{m}$ slightly deviates from the degeneracy direction, circular polarization becomes elliptic. We study the rotation of polarization ellipses when the wave normal goes around this degeneracy using the example of a crystal with a symmetry plane, which was investigated in Section 4.1 (see Fig. 8). The presence of the symmetry simplifies and clarifies the analysis, preserving the generality of final conclusions. Our discussion still applies to both acoustics and optics.

Let the wave normal $\mathbf{m}$ go around the singular axis $\mathbf{m}_0^+$ along a small contour Γ (Fig. 11). As in (32), we have

$$\Delta\mathbf{m} = \Delta\mathbf{m}_0 + \chi\mathbf{t}(\theta)\,, \tag{65}$$

where χ is a dimensionless small parameter and the vector $\mathbf{t}(\theta)$ draws a closed finite contour as θ changes form 0 to 2π. According to the laws of topology, the magnitude of rotation of polarization ellipses in going around the full contour is independent of its shape. This allows optimizing the analysis by selecting the contour shape. In our case, it is convenient to select the contour Γ in the form of an ellipse with the semiaxes equal to χ along $\mathbf{q}$ and $\chi q/p$ along $\mathbf{p}$:

$$\mathbf{t} = \frac{\mathbf{q}}{q}\cos\theta - \frac{\mathbf{q}\times\mathbf{m}_0}{p}\sin\theta \tag{66}$$

(see Fig. 11). In optics, when $q/p = 1$, the contour Γ becomes a circle (Fig. 3b).

As before, the value of χ must be small compared to the vector length $|\Delta\mathbf{m}_0| = p''/q$. This allows introducing a new smallness parameter:

$$\varepsilon = \frac{\chi}{|\Delta\mathbf{m}_0|} = \frac{\chi q}{p''} \ll 1\,. \tag{67}$$

Substituting (27), (65), and (66) in expressions (40) and taking into account that $\mathbf{pq} = 0$, $g = \mathbf{p}(\mathbf{q}\times\mathbf{m}_0) = pq\operatorname{sgn} g$, and $q'' = 0$ in the case under study, we obtain

$$\begin{aligned} &f \approx \mathrm{i}\left[1 - \varepsilon\exp\left(\mathrm{i}\tilde{\theta}\right)\right], \qquad Q \approx \sqrt{2\varepsilon}\,\exp\frac{\mathrm{i}\tilde{\theta}}{2}\,,\\ &f \pm Q \approx \mathrm{i} \pm \sqrt{2\varepsilon}\,\exp\frac{\mathrm{i}\tilde{\theta}}{2}\,,\\ &\Theta_\pm \approx \frac{1}{4}(\tilde{\theta}\pm\pi) \mp \sqrt{\frac{\varepsilon}{2}}\cos\frac{\tilde{\theta}}{2}\,, \end{aligned} \tag{68}$$

where

$$\tilde{\theta} \equiv \theta\operatorname{sgn} g\,. \tag{69}$$

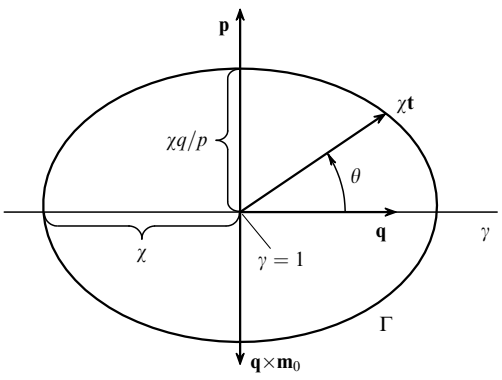

Figure 11. Contour Γ around the $\mathbf{m}_0^+$ axis on the $\mathbf{m}^2 = 1$ unit direction sphere in the $\{\mathbf{p},\mathbf{q}\}$ plane (the vector $\mathbf{p}$ is shown in the case $g < 0$).

These relations, together with expression (39), specify the polarization vectors $\mathbf{A}_{1,2}$ of isonormal waves on the contour Γ in the first order in $\sqrt{\varepsilon}$:

$$\begin{aligned} \mathbf{A}_{1,2} = \frac{1}{\sqrt{2}}\Bigg\{&(\mathbf{A}_{01} + \mathrm{i}\mathbf{A}_{02})\exp\left(-\mathrm{i}\,\frac{\tilde{\theta}\pm\pi}{4}\right)\\ &\pm\sqrt{\frac{\varepsilon}{2}}(\mathbf{A}_{02} + \mathrm{i}\mathbf{A}_{01})\exp\left(\mathrm{i}\,\frac{\tilde{\theta}\mp\pi}{4}\right)\Bigg\} \equiv \mathbf{A}'_{1,2} + \mathrm{i}\mathbf{A}''_{1,2}\,. \end{aligned} \tag{70}$$

We do not explicitly separate the real and imaginary parts. We can easily verify that major semiaxes $\mathbf{A}'_{1,2}$ and $\mathbf{A}''_{1,2}$ of the polarization ellipses of isonormal waves are mutually orthogonal and their lengths differ by terms of the order of $\sqrt{\varepsilon}$. It is also easy to verify that after going around the full contour Γ, the polarization vectors transform as

$$\mathbf{A}_1(\tilde{\theta}+2\pi) = -\mathbf{A}_2(\tilde{\theta})\,, \qquad \mathbf{A}_2(\tilde{\theta}+2\pi) = \mathbf{A}_1(\tilde{\theta})\,. \tag{71}$$

Therefore, after the wave normal $\mathbf{m} = \mathbf{m}_0^+ + \chi\mathbf{t}(\theta)$ completely goes around the $\mathbf{m}_0^+$ axis, each of the ellipses rotates through the angle $\pi/2$, transforming into the initial ellipse of another isonormal wave. However, for a combination of these conjugate ellipses after going around a closed contour, a pair of polarizations of two branches identically transform into themselves. It follows from (69) and (70) that the rotation directions of the vector $\mathbf{t}$ in the $\{\mathbf{p},\mathbf{q}\}$ plane and the vectors $\mathbf{A}_{1,2}$ in the $\{\mathbf{A}_{01},\mathbf{A}_{02}\}$ plane are the same for $g > 0$ and opposite for $g < 0$.

Such an orientational singularity is characterized by the Poincaré index [12, 16]

$$n = \frac{1}{4}\operatorname{sgn} g\,, \tag{72}$$

which is defined as the total rotation of the polarization ellipse (in 2π units) after completely going around the degeneracy point. Of course, the index of the second singular axis $\mathbf{m}_0^-$ is equal to the same value (72). This already follows from the fact that the $\mathbf{m}_0^+$ and $\mathbf{m}_0^-$ axes are separated by the symmetry plane (see Fig. 8). We note, however, that the identity of the indices of split axes is also preserved in a triclinic crystal [16]. We do not demonstrate this here.

From Fig. 12, where the picture of orientational singularities for split axes is presented, we see that after going around each of the points $\mathbf{m}_0^+$ and $\mathbf{m}_0^-$, pairs of polarization ellipses rotate through a quarter-turn, irrespective of the contour shape. The ellipticity value can change with a broadening of the contour, but the Poincaré index does not change. However, this occurs until two degeneracy points are both within the contour. After that instant, the total turn of a pair of ellipses increases jumpwise up to a half-turn, corresponding to the total Poincaré index $n = 1/4 + 1/4 = 1/2$.

For the rotation of polarization ellipses considered here, the passage through an equal-velocity line and an equal-absorption line involves the exchange of branches: the ellipses 'pass' from one sheet to another. Such a continuous passage between the external and internal sheets of the slowness and absorption surfaces when completely going around the singularity axis is shown in Fig. 4a. The physical identity of polarization pictures at points θ and $\theta + 2\pi$ is realized in the combined field of two branches rather than due to the coincidence of wave characteristics within each of the branches, as in nonabsorbing crystals. This became possible because of the new topological property of wave surfaces, their self-intersection along lines (see Figs 4–6).

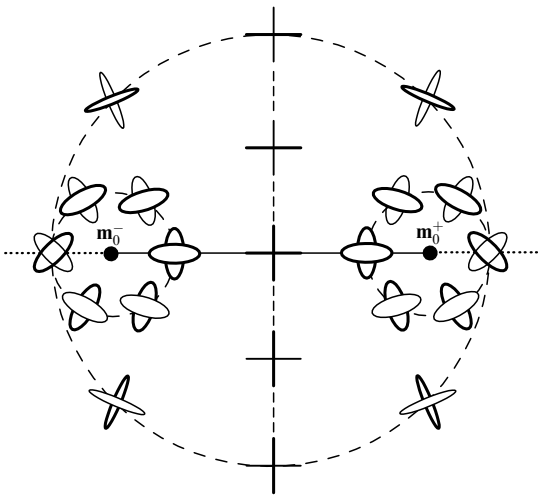

Figure 12. Elliptic polarization field in the vicinity of singular $\mathbf{m}_0^{\pm}$ axes of an absorptive crystal for $g > 0$, $n = 1/4$ on small contours around split degeneracy points. The total index $n = 1/2$ on the external contour coincides with the index of the unperturbed linear polarization field around the initial degeneracy direction of a nonabsorbing crystal. The dashed vertical straight line corresponds to linear polarization. A thicker contour of an ellipse corresponds to a higher velocity; absorption is higher for an ellipse drawn over another ellipse.

In the absence of absorption, the sheets of the velocity surface usually have only contact points (see Fig. 2a, which applies to optics). Polarizations of isonormal waves near such a point can be conventionally represented by a cross, with the fragments forming it being orthogonal and having the same length but different thicknesses, because one of the two isonormal waves on any contour around the degeneracy direction is always faster than the other. When absorption is neglected, a pair of singular axes collapses into one, and the ellipses on the external contour in Fig. 12 transform into such crosses. To make a cross coincident with itself, it is necessary to turn it through the minimum angle $\pm\pi$, which corresponds to the index $n = \pm 1/2$.

In optics, negative Poincaré indices do not appear. We recall that according to (28), the factor g is always positive in optics: $g = (\lambda v_0)^2$. Because of this, expression (72) gives only one value, $n = 1/4$, of the index of a singular optical axis in an absorptive crystal. This result was first obtained in [9] (see also [10, 11]). A singularity in the polarization field near the optical axis in a transparent biaxial crystal has the Poincaré index $n = 1/2$. The decomposition of such a singularity into two singularities with the indices $n = 1/4$ caused by the inclusion of absorption satisfies the law of conservation of topological charges (see Fig. 12).

The patterns of topological singularities in the acoustics of crystals are more diverse. In particular, unlike in optics, the Poincaré indices of polarization singularities can have different signs [12, 16, 17]. For example, during propagation along a conical acoustic axis parallel to symmetry axis 3, we always have $n = -1/2$. During propagation along a tangential acoustic axis parallel to symmetry axis 6 (the only optical axis in the optics of uniaxial crystals), we always have $n = 1$. But along symmetry axis 4, which is also a tangential acoustic axis, the index $n = -1$ is also possible along with the Poincaré index $n = 1$ [17]. Almost all acoustic axes in directions not coinciding with the symmetry axes of a crystal are conical and have Poincaré indices $n = \pm 1/2$. It is these axes that are split into pairs of singular axes characterized by the indices $n = \pm 1/4$ (72).

4.3 Rotation of real polarization vectors along elliptical trajectories

We now discuss the kinematics of polarization vectors of isonormal waves moving along elliptic trajectories. For this, we need a new time-dependent real characteristic

$$\boldsymbol{\mathcal{A}}_{1,2} = \operatorname{Re}\left[\mathbf{A}_{1,2}\exp\left(\mathrm{i}\Phi_{1,2}\right)\right], \qquad \Phi_{1,2} = k'_{1,2}\mathbf{mr} - \omega t, \quad (73)$$

instead of the complex vector $\mathbf{A}_\alpha$. We recall that the isonormal waves described here are independent, and the time origin in their phases $\Phi_{1,2}$ is selected arbitrarily. Taking this into account and applying procedure (73) to general expression (39), we can easily obtain that

$$\begin{aligned}\boldsymbol{\mathcal{A}}_{1,2} = {} & \mathbf{A}_{01}\cos\beta_\pm\cos\left(\Phi_{1,2} - \alpha_\pm\right) \\ & + \mathbf{A}_{02}\sin\beta_\pm\cos\left(\Phi_{1,2} + \alpha_\pm\right), \end{aligned} \quad (74)$$

where the angles $\beta_\pm$ and $\alpha_\pm$ are defined by the relations

$$\tan\beta_\pm = |f \pm Q|, \qquad \alpha_\pm = \frac{1}{2}\arg\left(f \pm Q\right). \quad (75)$$

The real part of a generalized wave $\mathbf{a}_\alpha(\mathbf{r}, t)$ in (12) [elastic $\mathbf{u}_\alpha(\mathbf{r}, t)$ in (2) or electromagnetic $\mathbf{h}_\alpha(\mathbf{r}, t)$ in (4)] can be written in terms of the polarizations $\boldsymbol{\mathcal{A}}_\alpha$ in (73) as

$$\operatorname{Re}\mathbf{a}_\alpha(\mathbf{r}, t) = C\boldsymbol{\mathcal{A}}_\alpha\exp\left(-k''\mathbf{mr}\right). \quad (76)$$

Here, the trivial effect of absorption related to the attenuation of a wave during its propagation is separated from the fundamentally different effects discussed in this paper.

In what follows, we are specifically interested in the change in the kinematics of rotation of the vectors $\boldsymbol{\mathcal{A}}_{1,2}$ along polarization ellipses when the wave normal scans the self-intersection line γ of wave surfaces both between singular axes, $|\gamma| < 1$, and in equal-absorption regions $|\gamma| > 1$. To avoid cumbersome expressions, we still consider a crystal with a symmetry plane in the geometry presented in Fig. 8.

First, we find real polarizations $\boldsymbol{\mathcal{A}}_{1,2}$ corresponding to the vectors $\mathbf{A}_{1,2}$ in (62) and (63):

$$\left.\begin{aligned}\boldsymbol{\mathcal{A}}_1 &= \mathbf{A}_{01}\sin\frac{\xi}{2}\sin\Phi_\xi + \mathbf{A}_{02}\cos\frac{\xi}{2}\cos\Phi_\xi, \\ \boldsymbol{\mathcal{A}}_2 &= \mathbf{A}_{01}\cos\frac{\xi}{2}\cos\Phi_\xi - \mathbf{A}_{02}\sin\frac{\xi}{2}\sin\Phi_\xi\end{aligned}\right\} \quad |\gamma| < 1, \quad (77)$$

$$\begin{aligned}\boldsymbol{\mathcal{A}}_{1,2} = {} & \frac{1}{\sqrt{2}}\left[\left(\mathbf{A}_{01} \pm \mathbf{A}_{02}\right)\cos\frac{\zeta}{2}\cos\Phi_\zeta\right. \\ & \left. - \left(\mathbf{A}_{02} \mp \mathbf{A}_{01}\right)\sin\frac{\zeta}{2}\sin\Phi_\zeta\right] \\ = {} & \frac{1}{\sqrt{2}}\left[\mathbf{A}_{01}\cos\left(\frac{\zeta}{2} \mp \Phi_\zeta\right) \pm \mathbf{A}_{02}\cos\left(\frac{\zeta}{2} \pm \Phi_\zeta\right)\right], \quad |\gamma| > 1. \end{aligned} \quad (78)$$

The indices ξ and ζ at the phases Φ in (77) and (78) mean that wave normals present in them scan certain parts of the self-intersection line γ:

$$\mathbf{m}_\xi = \mathbf{m}_0 + |\Delta\mathbf{m}_0|\sin\xi, \qquad \mathbf{m}_\zeta = \mathbf{m}_0 + |\Delta\mathbf{m}_0|\operatorname{cosec}\zeta. \quad (79)$$

We note that the phases Φ_ξ and Φ_ζ contain parameters $k'_{1,2}$, Eqn (73), which are identical on the line γ between the axes

($|\gamma| \leqslant 1$), but different outside the wedge edge ($|\gamma| > 1$). Therefore, for the same choice of the time origin, the phases Φ_ξ are independent of the wave branch number, whereas the phases Φ_ζ are different for two isonormal waves due to different $k'_{1,2}$.

Expressions (77) and (78) parametrically define two pairs of orthogonal polarization ellipses along which the vectors $\boldsymbol{\mathcal{A}}_{1,2}$ run for the wave period. The first pair has semiaxes $|\sin\xi/2|$ and $|\cos\xi/2|$ oriented along the coordinate vectors $\mathbf{A}_{01}$ and $\mathbf{A}_{02}$, while the second pair with semiaxes $|\sin\zeta/2|$ and $|\cos\zeta/2|$ is turned with respect to the first one through $\pi/4$, which corresponds to our analysis in Section 4.2. As the line γ is scanned by the wave normal from the wedge center $\xi = 0$ to the singular axis $\xi = \pm\pi/2$, the ellipticity increases from zero to unity (i.e., changes from linear to circular). After passing through the point $\xi = \zeta = \pm\pi/2$, the orientation of a pair of ellipses changes jumpwise by $\pi/4$ and ellipticity (61) begins to decrease with decreasing $|\zeta|$ (with increasing $|\gamma|$) as $|\tan\zeta/2|$ (see the polarization distribution along the horizontal line passing through the degeneracy points $\mathbf{m}_0^\pm$ in Fig. 12).

The motion of the radius vectors $\boldsymbol{\mathcal{A}}_\alpha$ ($\alpha = 1, 2$) over polarization ellipses can be conveniently described in polar coordinates $(\mathcal{A}_\alpha, \varphi_\alpha)$:

$$\boldsymbol{\mathcal{A}}_\alpha = \mathcal{A}_\alpha(\mathbf{A}_{01}\cos\varphi_\alpha + \mathbf{A}_{02}\sin\varphi_\alpha)\,. \tag{80}$$

As a point moves along a fixed elliptic trajectory, the lengths $\mathcal{A}_\alpha$ of the radius vectors vary consistently with the azimuth φ_α. The radial and azimuthal motions play different roles, depending on the ellipse shape. In the case of a small ellipticity, obviously, radial (quasivibrational) motions dominate, whereas for a nearly circular polarization, the kinematics are mainly determined by the azimuthal component.

General expression (74) for the real polarization of a pair of isonormal waves propagating in a triclinic crystal in an arbitrary direction $\mathbf{m}$ in the vicinity of split degeneracies in polar coordinates has standard form (80), where

$$\mathcal{A}_{1,2} = \sqrt{\cos^2\beta_\pm\cos^2(\Phi_{1,2} - \alpha_\pm) + \sin^2\beta_\pm\cos^2(\Phi_{1,2} + \alpha_\pm)}\,, \tag{81}$$

$$\tan\varphi_{1,2} = \tan\beta_\pm\,\frac{\cos(\Phi_{1,2} + \alpha_\pm)}{\cos(\Phi_{1,2} - \alpha_\pm)}\,. \tag{82}$$

Returning to a simpler case of the crystal with a symmetry plane (see Fig. 8), where the observation point lies on the line γ containing degeneracy directions $\mathbf{m}_0^\pm$, we obtain the polar coordinates of the vectors $\boldsymbol{\mathcal{A}}_{1,2}$ in (77) and (78) in the more compact form

$$\left.\begin{aligned} &\mathcal{A}_{1,2} = \sqrt{\frac{1}{2}(1 + \cos\xi\cos 2\Phi_\xi)}\,,\\ &\tan\varphi_1 = \cot\frac{\xi}{2}\cot\Phi_\xi\,,\\ &\tan\varphi_2 = -\tan\frac{\xi}{2}\tan\Phi_\xi \end{aligned}\right\} \quad |\gamma| \leqslant 1\,, \tag{83}$$

$$\left.\begin{aligned} &\mathcal{A}_{1,2} = \sqrt{\frac{1}{2}(1 + \cos\zeta\cos 2\Phi_\zeta)}\,,\\ &\tan\varphi_{1,2} = \pm\frac{\cos(\zeta/2 \pm \Phi_\zeta)}{\cos(\zeta/2 \mp \Phi_\zeta)} \end{aligned}\right\} \quad |\gamma| \geqslant 1\,. \tag{84}$$

Differentiating expressions (83) and (84) with respect to time, we find the radial ($\dot{\mathcal{A}}_{1,2}$) and angular ($\dot\varphi_{1,2}$) velocities of motion of the ends of $\boldsymbol{\mathcal{A}}_{1,2}$ on the line γ:

$$\dot{\mathcal{A}}_{1,2} = \frac{\omega\cos\xi\sin 2\Phi_\xi}{\sqrt{2(1 + \cos\xi\cos 2\Phi_\xi)}}\,,$$
$$\dot\varphi_{1,2} = \frac{\omega\sin\xi}{1 + \cos\xi\cos 2\Phi_\xi}\,, \quad |\gamma| \leqslant 1\,, \tag{85}$$

$$\dot{\mathcal{A}}_{1,2} = \frac{\omega\cos\zeta\sin 2\Phi_\zeta}{\sqrt{2(1 + \cos\zeta\cos 2\Phi_\zeta)}}\,,$$
$$\dot\varphi_{1,2} = \frac{\omega\sin\zeta}{1 + \cos\zeta\cos 2\Phi_\zeta}\,, \quad |\gamma| \geqslant 1\,. \tag{86}$$

Here, we took into account that $\dot\Phi_\alpha = -\omega$, Eqn (73). We note that the period of these velocities is half the wave period. This reflects the fact that all the physically different situations are already exhausted after the half-turn of the nondirectional polarization vector.

The sectorial motion velocities are described by even simpler expressions. By definition, they are equal to the area swept by the radius vectors $\boldsymbol{\mathcal{A}}_{1,2}$ per unit time:

$$v_{1,2}^{\text{sec}} = \frac{1}{2}\,\mathcal{A}_{1,2}^2\,\dot\varphi_{1,2} = \frac{1}{4}\begin{cases}\omega\gamma\,, & |\gamma| \leqslant 1\,,\\ \dfrac{\omega}{\gamma}\,, & |\gamma| \geqslant 1\,.\end{cases} \tag{87}$$

These velocities are the same for both isonormal waves and are time-independent, being dependent only on the coordinate γ on the self-intersection line. The time independence of the sectorial velocity of polarization vectors of elliptically polarized waves was pointed out already in [6]. This general property appears only due to the ellipticity and is not necessarily related to absorption.

The sectorial velocity v_α^{sec} in (87) vanishes at the wedge center for $\gamma = 0$ ($\xi = 0$), where polarization becomes linear (see Fig. 12). The value of v_α^{sec} increases proportionally to γ with the distance from the center, reaches the maximum $v_\alpha^{\text{sec}} = \omega/4$ at $\gamma = \pm 1$, and then slowly decreases proportionally to $1/\gamma$. It follows from (87) that the vectors $\boldsymbol{\mathcal{A}}_{1,2}$ pass at a large angular velocity $\dot\varphi_{1,2}$ through the part of the trajectory at which their lengths $\mathcal{A}_{1,2}$ are small, and at a small angular velocity, through the part of the trajectory where their lengths are large (i.e., the respective vicinities of the minor and major semiaxes of polarization ellipses). Because these ellipses for isonormal waves are mutually orthogonal, the points of the extremal angular velocity $\dot\varphi_{1,2}$ occupy fixed positions on polarization ellipses, corresponding to orthogonal radius vectors $\boldsymbol{\mathcal{A}}_{1,2}$. This is not affected by the independence of the phases $\Phi_{1,2}$ and by the arbitrary choice of the time origin in them.

It follows from (85) and (86) that during the propagation of waves along singular axes for $\gamma = \pm 1$ ($\xi = \pm\pi/2$), when isonormal polarization ellipses merge into one circle $\boldsymbol{\mathcal{A}}_0$, the circular motion has a constant angular velocity $\dot\varphi_1 = \dot\varphi_2 = \pm\omega$. Here, the upper and lower signs correspond to rotation directions at the points $\xi = \pm\pi/2$. As the observation point moves away from singular axes to both sides, polarization ellipses gradually elongate (see Fig. 12). Accordingly, rotation of the vectors $\boldsymbol{\mathcal{A}}_{1,2}$ along these ellipses becomes less uniform. For $|\gamma| \ll 1$, the azimuthal angles $\varphi_{1,2}$ in (83) remain almost fixed (near major semiaxes) during half the period and then sharply change by 180°:

$$\tan\varphi_1 \approx \frac{2\cot\Phi_\xi}{\xi}\,, \qquad \tan\varphi_2 \approx -\frac{1}{2}\,\xi\tan\Phi_\xi\,.$$

Evidently, the instant of this jump depends on the phase Φ_ξ. Of course, no singularity of motion occurs as $\xi \to 0$. Simply, all kinematics is more and more determined by the radial motion component $\mathcal{A}_{1,2} \approx |\cos \Phi_\xi|$. As follows from (83) and (85), the motion becomes purely vibrational at $\xi = 0$.

5. Conical refraction in absorptive crystals

If a circularly polarized electromagnetic wave is incident normally on the boundary of a transparent biaxial crystal such that the boundary is perpendicular to the optical axis, then a cone of rays appears in the crystal. This phenomenon, called the internal conical refraction in crystal optics [1, 7, 22, 23], has been known since the 19th century. The origin of this cone is related to a conical contact point between the sheets of the surface of refraction along the optical axis in a transparent crystal (Fig. 2a). Normals to the surface at the contact point of the sheets form a cone of refraction rays. Obviously, such refraction cannot exist in uniaxial crystals, where the contact between sheets is tangential.

Similar considerations are also valid for conical refraction in acoustics [24–28], which was theoretically predicted and experimentally observed in cubic Ni crystals [24]. The most comprehensive theory of this effect in the case of an arbitrary elastic anisotropy is presented in [26] (also see [6]). Absorption leads to new features of conical refraction, which are analyzed for crystal acoustics in [16].

This phenomenon in the optics and acoustics of nonabsorbing crystals is caused, first of all, by the conical shape of the refraction surface and the orthogonality of the ray velocity to this surface. Absorption, as we showed, considerably complicates the geometry of the contact of refraction sheets, eliminating the conical point. In addition, we show in Section 5.3 that the orthogonality of the ray velocity to this surface, strictly speaking, disappears. It is therefore important to generalize the theory of conical refraction taking absorption into account for acoustics and optics simultaneously, using the developed universal formalism.

5.1 Ray velocities in the acoustics and optics of absorptive crystals

In this section, we use the concepts of the Umov–Poynting vector and the ray velocity of a wave. Introducing these quantities for absorptive crystals requires some care. We discuss the case of acoustics as an example. Multiplying equation of motion (1) by $\dot{u}_i$, we obtain two exact relations in the left- and right-hand sides:

$$\rho \dot{u}_i \ddot{u}_i = \frac{\mathrm{d}}{\mathrm{d}t}\left(\frac{1}{2}\,\rho \dot{u}_i^2\right), \tag{88}$$

$$\dot{u}_i(c_{ijkl}\,u_{l,kj} + \eta_{ijkl}\,\dot{u}_{l,kj}) = \frac{\mathrm{d}}{\mathrm{d}x_j}\left\{\dot{u}_i(\sigma_{ij} + \sigma'_{ij})\right\} - \frac{\mathrm{d}}{\mathrm{d}t}\left[\frac{1}{2}\,u_{i,j}\,c_{ijkl}\,u_{l,k}\right] - \dot{u}_{i,j}\,\eta_{ijkl}\,\dot{u}_{l,k}\,. \tag{89}$$

Combining these equations, we arrive at the continuity equation (energy balance),

$$-\frac{\mathrm{d}}{\mathrm{d}t}\,W = \operatorname{div}\mathbf{P} + D\,, \tag{90}$$

where

$$W = W_{\mathrm{kin}} + W_{\mathrm{el}} = \frac{1}{2}\,\rho \dot{u}_i^2 + \frac{1}{2}\,u_{i,j}\,c_{ijkl}\,u_{l,k} \tag{91}$$

is the total density of kinetic and elastic energies in the wave,

$$D = \dot{u}_{i,j}\,\eta_{ijkl}\,\dot{u}_{l,k} \tag{92}$$

is the energy dissipation per unit time, $\mathbf{P}$ is the energy flux in the wave (the Umov–Poynting vector),

$$P_j = -\dot{u}_i(\sigma_{ij} + \sigma'_{ij})\,, \tag{93}$$

and the tensors σ_{ij} and σ'_{ij} are defined by the contractions

$$\sigma_{ij} = c_{ijkl}\,u_{l,k}\,, \qquad \sigma'_{ij} = \eta_{ijkl}\,\dot{u}_{l,k}\,. \tag{94}$$

By definition, the ray velocity of the wave is $\mathbf{s} = \mathbf{P}/W$. With the general expressions (93) and (91) found for the energy flux and the total energy density, the exact expression for the ray velocity in an absorptive crystal becomes

$$s_j = -\frac{\dot{u}_i(c_{ijkl}\,u_{l,k} + \eta_{ijkl}\,\dot{u}_{l,k})}{(1/2)\,\rho \dot{u}_i^2 + (1/2)u_{i,j}\,c_{ijkl}\,u_{l,k}}\,. \tag{95}$$

Comparing (95) with the usual expression for a nonabsorbing crystal, we see that the numerator in (95) contains an additional term proportional to the viscosity. The denominator has a more customary form, but also contains similar additions in the displacement field itself. This is expressed, in particular, in the fact that the elastic energy differs somewhat from the kinetic energy, depending on the absorption intensity.

However, the following must be borne in mind. It is shown in Section 4.1 that the polarization of waves in the vicinity of degeneracies drastically changes due to absorption. Linear polarization transforms into an elliptic one, the ellipticity not being weak despite weak absorption, and polarization can even become circular. Therefore, the main effect of absorption on ray velocities $\mathbf{s}$ is already manifested in the leading order, via the polarization vectors. Below, we always describe ray velocities taking this leading-order effect into account and neglecting small additions proportional to absorption.

Of course, we should substitute not complex expression (2) but its real part $\operatorname{Re}\mathbf{u}$ in quadratic forms in the displacement field $\mathbf{u}(\mathbf{r}, t)$ in (95), as in (73) and (76):

$$\operatorname{Re}\mathbf{u}(\mathbf{r}, t) = C\boldsymbol{\mathcal{U}}\exp\left(-k''\mathbf{mr}\right), \qquad \boldsymbol{\mathcal{U}} = \operatorname{Re}\left\{U\exp\left[\mathrm{i}\Phi(\mathbf{r}, t)\right]\right\}, \tag{96}$$

where the real polarization $\boldsymbol{\mathcal{U}}$ can be found by replacing $\boldsymbol{\mathcal{A}} \to \boldsymbol{\mathcal{U}}$ in universal expression (74),

$$\boldsymbol{\mathcal{U}} = \mathbf{A}_{01}\cos\beta_\pm\cos\left(\Phi_{1,2} - \alpha_\pm\right) + \mathbf{A}_{02}\sin\beta_\pm\cos\left(\Phi_{1,2} + \alpha_\pm\right). \tag{97}$$

For compactness of expressions, we omit isonormal wave indices at the vectors $\boldsymbol{\mathcal{U}}$ and $\mathbf{u}$ in this section. Displacement field (96), (97) satisfies equation of motion (1) in a crystal with an arbitrary anisotropy for propagation directions in the vicinity of split axes. We note that differentiating the exponential $\exp\left(-k''\mathbf{mr}\right)$ in the calculation of spatial derivatives of $\operatorname{Re}\mathbf{u}(\mathbf{r}, t)$ in (96) gives small terms proportional to k'', which can be neglected. In this approximation, in (95), we can substitute the real polarization $\boldsymbol{\mathcal{U}}(\mathbf{r}, t)$ given by (97) instead of the total field $\operatorname{Re}\mathbf{u}(\mathbf{r}, t)$, setting

$$\dot{\boldsymbol{\mathcal{U}}} = \frac{\partial\boldsymbol{\mathcal{U}}}{\partial\Phi}\,\dot{\Phi} = -\omega\overline{\boldsymbol{\mathcal{U}}}, \qquad \boldsymbol{\mathcal{U}}_{,i} = \frac{\partial\boldsymbol{\mathcal{U}}}{\partial\Phi}\,\Phi_{,i} = k' m_i\overline{\boldsymbol{\mathcal{U}}}, \tag{98}$$

where the vector $\overline{\boldsymbol{U}}$ is given by formula (97) with a phase shift:

$$\overline{\boldsymbol{U}} = \boldsymbol{U}\left(\Phi + \frac{\pi}{2}\right). \tag{99}$$

The phase shift (i.e., the shift of the time origin $t \to t - \pi/2\omega$) in (99), of course, does not principally change anything in our stationary problem, but shows that the ray velocity $\mathbf{s}_\alpha$ is delayed in phase with respect to the polarization $\boldsymbol{U}$ by $\pi/2$. Taking these remarks into account, we obtain from (95) that

$$\mathbf{s} = \frac{2v'\overline{\boldsymbol{U}}\left[(\hat{c} - \omega\hat{\eta})\mathbf{m}\right]\overline{\boldsymbol{U}}}{\rho v'^2\overline{\boldsymbol{U}}^2 + \overline{\boldsymbol{U}}(\mathbf{m}\hat{c}\mathbf{m})\overline{\boldsymbol{U}}}. \tag{100}$$

We now find relations between two terms in the denominator in (100), which are proportional to the kinetic and elastic energy densities in the wave. For this, we substitute the vector function $\overline{\boldsymbol{U}}(\mathbf{r}, t)$ in equation of motion (1), which must be satisfied by this function up to small corrections proportional to k'', and multiply the obtained result by $\overline{\boldsymbol{U}}$. This gives the important relation

$$\rho v'^2\overline{\boldsymbol{U}}^2 = \overline{\boldsymbol{U}}\left[\mathbf{m}(\hat{c} - \omega\hat{\eta})\mathbf{m}\right]\overline{\boldsymbol{U}} \approx \overline{\boldsymbol{U}}(\mathbf{m}\hat{c}\mathbf{m})\overline{\boldsymbol{U}}, \tag{101}$$

where we omitted the term proportional to the viscosity $\hat{\eta}$ in the right-hand side, which has the same smallness order as the terms $\sim k''$ omitted previously. In the leading approximation of interest to us, the kinetic and elastic energies therefore coincide, even in the region of anomalous ellipticity.

For the same reason, we can omit the second term $\propto \hat{\eta} \sim k''$ in the numerator in (100) and set $\mathbf{m} = \mathbf{m}_0 + \Delta\mathbf{m} \approx \mathbf{m}_0$ and $v'_\alpha \approx v_0$, because the size of the region considered here and variations of the phase velocity in it are also proportional to the absorption. Taking this into account, we can write the ray velocity of the elastic wave in the leading order in the form

$$\mathbf{s}_{\text{ac}} = \frac{\overline{\boldsymbol{U}}(\rho^{-1}\hat{c}\mathbf{m}_0)\overline{\boldsymbol{U}}}{v_0\overline{\boldsymbol{U}}^2}. \tag{102}$$

In optics, similarly and with the same accuracy, we obtain

$$\mathbf{s}_{\text{op}} = \frac{\boldsymbol{\mathcal{H}}\left[(-c^2\hat{e}\hat{\varepsilon}^{-1}\hat{e})\mathbf{m}_0\right]\boldsymbol{\mathcal{H}}}{v_0\boldsymbol{\mathcal{H}}^2}. \tag{103}$$

It follows that the ray velocities $\mathbf{s}$, along with other wave characteristics, are described in acoustics and in optics by the same expressions if correspondence relations (12) and (13) supplemented with $\overline{\boldsymbol{U}} \leftrightarrow \boldsymbol{\mathcal{H}}$ are taken into account. In Sections 5.2 and 5.3, staying in the framework of the unified formalism, we use the relation

$$\mathbf{s}_\alpha = \frac{\boldsymbol{\mathcal{A}}_\alpha(\hat{\Lambda}'\mathbf{m}_0)\boldsymbol{\mathcal{A}}_\alpha}{v_0\boldsymbol{\mathcal{A}}_\alpha^2}, \tag{104}$$

in which additional phase shift (99) is assumed for acoustics.

5.2 Universal refraction cones in acoustics and optics

According to the original formulation of the problem, in the absence of absorption along the direction $\mathbf{m}_0$, conical degeneracy occurs and waves with any polarization, in particular, with the circular polarization $\mathbf{A} = (\mathbf{A}_{01} \pm \mathrm{i}\mathbf{A}_{02})/\sqrt{2}$, can propagate in the degeneracy plane D (see Fig. 1). In this case, expression (73) gives

$$\begin{aligned} &\boldsymbol{\mathcal{A}}_0 = \frac{1}{\sqrt{2}}(\mathbf{A}_{01}\cos\Phi_0 \mp \mathbf{A}_{02}\sin\Phi_0), \\ &\Phi_0 = k\mathbf{m}_0\mathbf{r} - \omega t. \end{aligned} \tag{105}$$

Substituting the expression for $\boldsymbol{\mathcal{A}}_0$ in (104) and taking (19) into account, we obtain the ray velocity

$$\mathbf{s}(t) = \mathbf{s}^0 + \tilde{\mathbf{s}}(t), \qquad \tilde{\mathbf{s}} = \mathbf{p}\cos 2\Phi_0 \mp \mathbf{q}\sin 2\Phi_0. \tag{106}$$

This is the classical picture of conical refraction along the acoustic/optical axis $\mathbf{m}_0$ in a nonabsorbing crystal. According to (106), during the wave period, the ray velocity vector $\mathbf{s}(t)$ runs over the refraction cone twice (Fig. 13) and the vector $\tilde{\mathbf{s}}(t)$ runs over the elliptic/circular section of this cone in the plane orthogonal to the vector $\mathbf{m}_0$.

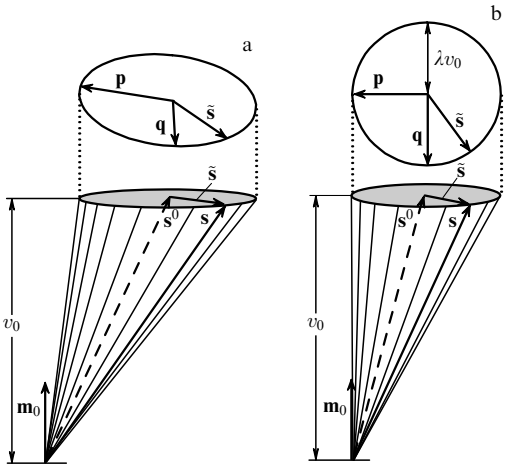

Figure 13. Universal refraction cones in (a) the acoustics and (b) the optics of absorptive crystals. Shown are the universal motion trajectories of the ends of the vectors $\tilde{\mathbf{s}}$.

We recall that the inclusion of absorption splits the degeneracy direction $\mathbf{m}_0$ into two singular directions $\mathbf{m}_0^+$ and $\mathbf{m}_0^-$ (Fig. 4b). The polarization of isonormal waves in the vicinity of these axes is characterized by ellipticity, which can be quite high and strongly dependent on the wave normal direction $\mathbf{m}$. The most general expressions in the case of an arbitrary anisotropy are given by (80)–(82). Using these expressions and (104), we can readily find the required ray velocities. Similarly to (106), we have

$$\begin{aligned} &\mathbf{s}_{1,2}(\mathbf{m}, t) = \mathbf{s}^0 + \tilde{\mathbf{s}}_{1,2}(\mathbf{m}, t), \\ &\tilde{\mathbf{s}}_{1,2}(\mathbf{m}, t) = \mathbf{p}\cos 2\varphi_{1,2} + \mathbf{q}\sin 2\varphi_{1,2}, \end{aligned} \tag{107}$$

where polar angles $\varphi_\alpha(\mathbf{m}, t)$ are determined by Eqn (82). It is easy to see that expressions (106) and (107) describe the precession of ray velocities over the same cone.

Thus, the inclusion of absorption extends the existence region of conical refraction from the local direction $\mathbf{m}_0$ to a whole continuum region in the vicinity of split axes. Here, we should not be misled by the fact that expression (104) for the ray velocity $\mathbf{s}$ related to the whole region around singular axes explicitly contains the wave normal $\mathbf{m}_0$ instead of $\mathbf{m}$. This only reflects the fact that the operator $\hat{\Lambda}'\mathbf{m}$ weakly depends on small variations of $\mathbf{m}$ and can be replaced by the operator $\hat{\Lambda}'\mathbf{m}_0$ in the leading approximation. The high sensitivity of the

ray velocity to small variations of the direction $\mathbf{m}$ in the region under study is related to the polarization $\boldsymbol{\mathcal{A}}(\mathbf{m}, t)$, which, as we saw, can change from circular to linear with small variations of $\mathbf{m}$.

Expressions (106) and (107) differ by the phases $\Phi_0(\mathbf{m}_0, t)$ and $\varphi_{1,2}(\mathbf{m}, t)$. The first phase, locked in the fixed direction $\mathbf{m}_0$, has simple time dependence (105). The second phase, being the polar azimuth of the polarization vector $\boldsymbol{\mathcal{A}}(\mathbf{m}, t)$, has a much more complicated time dependence (82), which is quite sensitive to the wave normal direction $\mathbf{m}$. All this can considerably affect the precession kinematics of the vectors $\mathbf{s}_{1,2}$. However, the trajectories of their motion, described by (106) and (107) in a parametric form, are in fact identical. The vectors $\mathbf{p}$ and $\mathbf{q}$ in these formulas are the conjugate half-diameters of an ellipse drawn by the end of the vector $\tilde{\mathbf{s}}(t)$ with changing time t. The elliptical section of the cone by the $(\mathbf{p}, \mathbf{q})$ plane is universal, and its principal semiaxes $\mathbf{s}_\pm$ are independent of phases and are determined by the invariant combinations of the vectors $\mathbf{p}$ and $\mathbf{q}$ [6],

$$s_\pm^2 = \frac{1}{2}\left(\mathbf{p}^2 + \mathbf{q}^2 \pm \sqrt{(\mathbf{p}^2 + \mathbf{q}^2)^2 - 4(\mathbf{p} \times \mathbf{q})^2}\,\right), \qquad (108)$$
$$\mathbf{s}_+ \parallel \mathbf{p} \times (\mathbf{q} \times \mathbf{p}) - s_+ \mathbf{q}\,, \quad \mathbf{s}_- \parallel \mathbf{p} \times (\mathbf{q} \times \mathbf{p}) - s_- \mathbf{q}\,.$$

In acoustics, as mentioned in Section 5.1, the polar angles $\varphi_{1,2}$ in (82) should be replaced by the phase-shifted angles

$$\bar{\varphi}_{1,2} = \varphi_{1,2}\left(\Phi + \frac{\pi}{2}\right). \qquad (109)$$

In optics, phase shift (109) is absent, and the general picture is simpler and more symmetric. According to (23), the vectors $\mathbf{p}$ and $\mathbf{q}$ are then orthogonal and have equal lengths. As a result, the universal ellipse transforms into a circle lying in the $(\mathbf{A}_{01}, \mathbf{A}_{02})$ plane orthogonal to the vector $\mathbf{m}_0 = \mathbf{c}_\mathrm{I} = \mathbf{A}_{03}$. The center of the circle with the radius λv_0 is located at the point specified by the end of the vector $\mathbf{s}^0 = (-\lambda \mathbf{A}_{01} + \mathbf{A}_{03}) v_0$ in (23). The perpendicular to this plane drawn from the apex of the cone has the length v_0 and meets the circle at a point corresponding to the end of the vector $\mathbf{p} = \lambda v_0 \mathbf{A}_{01}$ (see Fig. 13b). Correspondingly, the cone opening angle ψ_c in the $\{\mathbf{A}_{01}, \mathbf{A}_{03}\}$ plane is determined by the equation

$$\tan \psi_\mathrm{c} = 2\lambda\,. \qquad (110)$$

The axes $\mathbf{s}^0$ of the acoustic and optical cones are tilted with respect to the direction $\mathbf{m}_0$, this tilt being independent of the absorption parameters in both cases. But, as shown in Section 2.3, in the absence of absorption in optics, the optical axis $\mathbf{m}_0 = \mathbf{c}_\mathrm{I}$ lies in the symmetry plane of the tensor $\hat{\varepsilon}$ (Fig. 2a). Therefore, the cone axis $\mathbf{s}^0$, inclining to $\mathbf{m}_0$, remains in the same plane. The inclusion of absorption restores the optical triclinity of the crystal, but this does not concern the refraction cone in the leading approximation used here. In acoustics, a triclinic crystal remains triclinic without absorption as well, and therefore the cone tilt is not connected to any selected planes. Of course, the inclusion of symmetry changes the situation in acoustics. For example, in a particular case where the degeneracy direction $\mathbf{m}_0$ coincides with symmetry axis 3, through which three symmetry planes always pass, the refraction cone not only becomes circular but also loses its tilt, because $\mathbf{s}^0 \parallel \mathbf{m}_0$. However, precisely due to the symmetry, the absorption does not split the acoustic axis $\mathbf{m}_0$ here [12, 16].

5.3 Precession kinematics of ray velocities

As mentioned in Section 5.2, the absorption intensity affects the kinematics of the ray velocity precession over the universal cone rather than the trajectory of ray velocity motion. These kinetics, in turn, strongly depend on the propagation direction $\mathbf{m}$ in the vicinity under study. A convenient characteristic of such precession can be the angular velocity of rotation of the vector $\tilde{\mathbf{s}}_\alpha(t)$ $(\alpha = 1, 2)$ over a circle in optics or over an ellipse in acoustics.

In the first case, by substituting expressions $\mathbf{p}_\mathrm{op} = \lambda v_0 \mathbf{A}_{01}$ and $\mathbf{q}_\mathrm{op} = \lambda v_0 \mathbf{A}_{02}$ from (23) in (107), we immediately obtain the final formula in polar coordinates:

$$\tilde{\mathbf{s}}_\alpha^\mathrm{op}(t) = \lambda v_0 (\mathbf{A}_{01} \cos 2\varphi_\alpha + \mathbf{A}_{02} \sin 2\varphi_\alpha)\,, \qquad (111)$$

where the polar angle is $\phi_\alpha^\mathrm{op} = 2\varphi_\alpha$.

In acoustics, because the vectors $\mathbf{p}$ and $\mathbf{q}$ are not orthogonal and have different lengths, the relation between the polar angle ϕ_α^ac and the angle $2\bar{\varphi}_\alpha$ is more complicated and can be found from the condition

$$\tilde{\mathbf{s}}_\alpha^\mathrm{ac}(t) = \mathbf{p} \cos 2\bar{\varphi}_\alpha + \mathbf{q} \sin 2\bar{\varphi}_\alpha$$
$$= S_\alpha \left(\frac{\mathbf{p}}{p} \cos \phi_\alpha^\mathrm{ac} + \frac{\mathbf{m}_0 \times \mathbf{p}}{p} \sin \phi_\alpha^\mathrm{ac}\right), \qquad (112)$$

where S_α is the length of the radius vector $\tilde{\mathbf{s}}_\alpha^\mathrm{ac}$. This gives

$$\cot \phi_\alpha^\mathrm{ac} = \frac{1}{g}(\mathbf{pq} + p^2 \cot 2\bar{\varphi}_\alpha), \quad \sin \phi_\alpha^\mathrm{ac} = \frac{g}{pS_\alpha} \sin 2\bar{\varphi}_\alpha\,, \qquad (113)$$

$$S_\alpha^2 = p^2 \cos^2 2\bar{\varphi}_\alpha + q^2 \sin^2 2\bar{\varphi}_\alpha + \mathbf{pq} \sin 4\bar{\varphi}_\alpha\,. \qquad (114)$$

With these relations, the angular precession velocities in optics and in acoustics are determined by the respective expressions

$$\dot{\phi}_\alpha^\mathrm{op} = 2\dot{\varphi}_\alpha\,, \qquad \dot{\phi}_\alpha^\mathrm{ac} = \frac{2g}{S_\alpha^2}\,\dot{\bar{\varphi}}_\alpha\,. \qquad (115)$$

Therefore, the angular precession velocity $\dot{\phi}_\alpha$ of $\mathbf{s}_\alpha(t)$ in both optics and acoustics is completely determined by the kinematics of the motion of the vector $\boldsymbol{\mathcal{A}}_\alpha$ over the polarization ellipse, which occurs in acoustics with the phase delay $\Phi_\alpha \to \Phi_\alpha + \pi/2$. The same concerns the sector velocity of the vector $\tilde{\mathbf{s}}_\alpha(t)$:

$$\bar{v}_\alpha^\mathrm{sec} = \frac{1}{2}\, S_\alpha^2 \dot{\phi}_\alpha = \begin{cases} g\dot{\varphi}_\alpha & (\mathrm{op})\,, \\ g\dot{\bar{\varphi}}_\alpha & (\mathrm{ac})\,. \end{cases} \qquad (116)$$

Unlike sector polarization velocity (87), velocity (116) is not constant and is phase-delayed in acoustics. In optics, we can set $g = (\lambda v_0)^2$ in (116). It hence follows that in optics, the rotation signs for the vector $\tilde{\mathbf{s}}_\alpha(t)$ and the corresponding vector $\boldsymbol{\mathcal{H}}_\alpha(t)$ always coincide with each other. In acoustics, the coincidence occurs only if $g > 0$. For $g < 0$, a possibility occurs that is forbidden in optics, when the rotation signs of the ray velocity and polarization are opposite.

We can see from expressions (115) that all the kinematic features of polarization rotation over ellipses discussed in Section 4.3 should also be reproduced in the precession of ray velocities. Along the singular axes, two conjugate polarization ellipses degenerate into a circle, producing circular polarization (50). Expressions (77) and (85) for $\xi = \pm\pi/2$ give the constant angular velocity $\dot{\varphi}_0 = \omega \operatorname{sgn} \xi$. This exactly corresponds to the kinematics of the usual conical refraction

in a nonabsorbing crystal, Eqn (106). In this case, absorption affects the geometry of the refraction surface rather than the kinematics. In the absence of absorption, the refraction cone completely repeats the orientation of the cone of normals to the slowness surface at the conical contact point of its sheets. If dissipation along the singular axis is taken into account, the cone of normals is replaced with their flat fan (Fig. 5a), while the refraction cone remains invariable. This illustrates the fact that under the conditions under study, the convenient correspondence between the directions of ray velocities and the normal to the refraction surface is unfortunately lost. However, the collinearity of these directions is completely restored on the zero-ellipticity line.

According to (115) and (116), along singular axes, where $\dot{\varphi}_\alpha = -\dot{\Phi}_\alpha \operatorname{sgn}\xi = \omega \operatorname{sgn}\xi$, both angular and sector velocities of ray vectors remain constant in optics:

$$\dot{\phi}_0^{\mathrm{op}} = 2\omega \operatorname{sgn}\xi\,, \qquad \bar{v}_0^{\mathrm{sec}} = g\omega \operatorname{sgn}\xi\,, \tag{117}$$

while only the sector velocity, determined by the same expression (117), remains constant in acoustics. Angular precession velocity (115) of the vectors $\mathbf{s}_{1,2}(t)$ during propagation along the singular acoustic axis continues to vary in time as long as the vectors $\mathbf{p}$ and $\mathbf{q}$ remain nonorthogonal and have different lengths.

However, as the observation point moves along the wedge edge from its ends to the center ($\xi = 0$), the nonuniformity of the motion of the vectors $\mathbf{s}_{1,2}(t)$ in terms of both angular and sector velocities rapidly increases. The same should take place on any observation point trajectory intersecting the zero-ellipticity line. As a result, the illumination of a screen should depend on the ellipticity of the wave for a given direction of the wave normal. In optics, the polarization of a wave propagating along the singular axis is circular and the precession of the ray $\mathbf{s}_\alpha(t)$ occurs at a constant angular velocity $\pm 2\omega$, Eqn (117). In this case, the screen illumination represents a completely drawn circle (Fig. 14).

As the 'observation point' moves away from singular axes, the illumination pattern ceases to be uniform. The parts of the refraction ellipse through which the vectors $\mathbf{s}_{1,2}(t)$ pass rapidly become less illuminated than the parts through which these vectors pass more slowly. The phase velocity of this motion $\dot{\phi}_\alpha^{\mathrm{op}} = 2\dot{\varphi}_\alpha$ in Eqn (115) is exactly twice the velocity of the polarization vector $\boldsymbol{\mathcal{A}}_\alpha$, which, as shown in Section 4.3, has extrema along the semiaxes of the polarization ellipse for $\varphi_\alpha = \varphi_\alpha^m$. The illumination regions of interest to us correspond to the vicinities of major semiaxes of these ellipses and are uniquely related to their orientations. The motion of the vector $\boldsymbol{\mathcal{A}}_\alpha(t)$ over one ellipse from one end position $\boldsymbol{\mathcal{A}}_\alpha(\varphi_\alpha^m) = \boldsymbol{\mathcal{A}}_\alpha$ to another, $\boldsymbol{\mathcal{A}}_\alpha(\varphi_\alpha^m + \pi) = -\boldsymbol{\mathcal{A}}_\alpha$, does not affect the orientation of the ray velocity, because according to (111), both these positions correspond to the same direction $\mathbf{s}_\alpha[2(\varphi_\alpha^m + \pi)] = \mathbf{s}_\alpha(2\varphi_\alpha^m)$, and therefore the additional illumination falls on the same place in the refraction ellipse, thereby enhancing the first illumination. Obviously, for the second isonormal wave, the extreme positions φ_2^m of the vector $\boldsymbol{\mathcal{A}}_2$ in its polarization ellipse, which is orthogonal to $\boldsymbol{\mathcal{A}}_1$, differ from the first ones by $\pi/2$, $\varphi_2^m = \varphi_1^m \pm \pi/2$. Therefore, they should correspond to the extreme ray velocity $\mathbf{s}_2(2\varphi_2^m) = \mathbf{s}_1(2\varphi_1^m \pm \pi)$ directed along the opposite generatrix of the refraction cone, which adds a new illumination region on the opposite side of the same refraction ellipse. On the zero-ellipticity line, precession completely disappears, in both optics and acoustics, and the screen illumination contour contains only two points corresponding to usual birefringence.

Such refraction circles with a double illumination from pairs of isonormal waves are shown in the case of optics in Fig. 14. The positions of illumination regions in circular contours correspond to orientations of polarization ellipses in Fig. 12. In the acoustics of absorptive crystals, the illumination pattern is similar, but the circle is replaced by an ellipse described by (107).

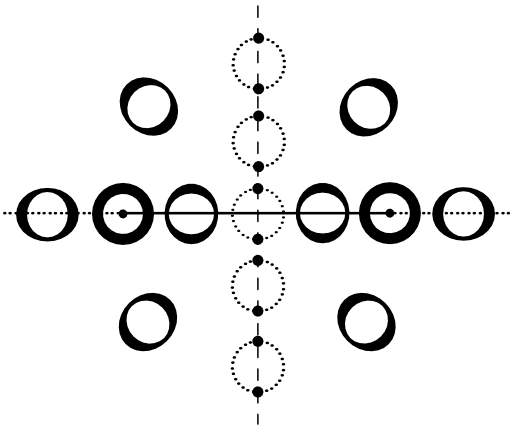

Figure 14. Schematic distribution of illumination rings on a screen in the vicinity of split singular axes in optics. The full uniform circular illumination of the screen corresponds to the usual circular refraction of circularly polarized waves. Two points on a circle correspond to the usual birefringence of linearly polarized waves. The edge of an equal-velocity wedge is shown by a segment of the horizontal straight line. The vertical dashed straight line corresponds to zero ellipticity.

6. Possibilities of observing topological absorption effects

We now discuss the prospects of experimental observations of the predicted subtle effects in optics and acoustics caused by the splitting of the optic and acoustic axes due to absorption. To observe these effects, the diffraction-limited divergence angle $\Delta\psi_{\mathrm{d}}$ of a probe wave beam should be smaller than the splitting angle $\Delta\Psi$ of the optical or acoustic axes. The divergence angle can be estimated from the relation

$$\Delta\psi_{\mathrm{d}} \sim \frac{\lambda_0}{d_0}\,, \tag{118}$$

where λ_0 is the wavelength in the vacuum and d_0 is the beam diameter in the crystal. The splitting angle $\Delta\Psi$ is controlled by the choice of the absorption level, which must nevertheless provide a large enough free path for the wave.

We begin with optics. According to (32) and (33), the splitting angle $\Delta\Psi$ (see Fig. 8) is estimated as

$$\Delta\Psi \approx 2|\Delta\mathbf{m}_0| \sim \frac{\varepsilon\delta}{2\lambda}\,. \tag{119}$$

Here, ε and δ are the characteristic values of the components $\hat{\varepsilon}$ and $\hat{\delta}$ of the absorption tensor, and the parameter λ, Eqn (23), is determined by optical anisotropy, which is small enough in most crystals. For example, λ is almost the same and quite small in topaz and Seignette salt crystals: $\lambda \approx 1.6 \times 10^{-3}$ [7].

In handbooks, absorption in crystals is usually specified not by components of the tensor $\hat{\delta}$ but by linear absorption coefficients k'' along the principal axes of the tensor $\hat{\varepsilon}$. In the

typical weak-anisotropy case, the relation between δ and k'' can be easily found:

$$k' + \mathrm{i}k'' \approx \frac{2\pi}{\lambda_0\sqrt{\varepsilon^{-1} - \mathrm{i}\delta}} \approx \frac{2\pi\sqrt{\varepsilon}}{\lambda_0}\left(1 + \mathrm{i}\,\frac{\varepsilon\delta}{2}\right). \qquad (120)$$

This gives

$$\delta \approx \frac{\lambda_0}{\pi\varepsilon^{3/2}}\,k''. \qquad (121)$$

Substituting this estimate in (119) and comparing the result with (118), we obtain the sought criterion for observing the splitting of optic axis and accompanying effects:

$$k''d_0 > 2\pi\lambda\sqrt{\varepsilon}. \qquad (122)$$

We see from (122) that in crystals with the weak anisotropy $\lambda \sim 10^{-3}$, the requirements imposed on the absorption level are rather weak: $k''d_0 > 10^{-2}$. For example, for $k'' \sim 1\ \mathrm{cm}^{-1}$, when the free path of the wave in a crystal is ~ 1 cm, the fulfillment of this condition is provided for reasonable values $d_0 \sim 3-5$ mm. However, we should bear in mind that the refraction cone opening angle (110) for small λ also decreases: $\psi_c \approx 2\lambda$ (for example, for $\lambda \approx 1.6 \times 10^{-3}$, we have $\psi_c \approx 0.2^\circ$), which can complicate experiments. We note that typical refraction cone angles ψ_c in acoustics are a few dozen degrees.

For example, taking $k'' \approx 1\ \mathrm{cm}^{-1}$ and $\lambda_0 \approx 5 \times 10^{-5}$ cm, we obtain the estimate $\delta \sim 10^{-5}$ from (121). For this value of δ and $\lambda \sim 10^{-3}$, expression (119) gives the splitting angle $\Delta\Psi \sim \delta/\lambda \sim 10^{-2} \sim 0.5^\circ$. For such a splitting of optical axes, the condition $\Delta\psi_d \ll \Delta\Psi$ imposed on the laser beam divergence can be easily satisfied. Hence, the predicted effects can be observed beyond any doubt in optics in properly chosen crystals.

In making similar estimates in acoustics, we take into account that absorption increases as the wave frequency $\nu = \omega/2\pi$ increases, and hence the angle $\Delta\Psi$ increases, while the beam divergence angle $\Delta\psi_d \sim c_s/\nu d_0$, on the contrary, decreases (here, c_s is the speed of sound in a crystal). In this case, the lower frequency threshold of the effect should therefore exist.

Taking expressions (13), (19), (20), (25), and (26) into account, we now have the estimate $\Delta\Psi \sim 2\pi\nu\eta/\mu$ instead of (119), where η is the viscosity parameter and μ is the shear modulus. As a result, the criterion

$$\nu \gg \nu_{th} \sim \sqrt{\frac{c_s\,\mu}{2\pi\eta d_0}} \qquad (123)$$

follows from the condition $\Delta\psi_d \ll \Delta\Psi$. Because we are dealing with rather high frequencies and room temperatures $T \sim 300$ K, the wave decay η can be naturally estimated by using the phonon viscosity

$$\eta \sim \eta_{ph} \sim \tau_{ph}\,\frac{3k_B T}{a^3}, \qquad (124)$$

where τ_{ph} is the phonon relaxation time, k_B is the Boltzmann constant, and a is the lattice constant. Substituting (124) in (123) with $c_s \approx 3 \times 10^5$ cm s^{-1}, $\mu \approx 10^{11}$ dyn cm^{-2}, $d_0 \approx 0.5$ cm, $\tau_{ph} \approx 10^{-10}$ s, and $a \approx 3 \times 10^{-8}$ cm, we estimate the threshold frequency as

$$\nu_{th} \sim 100\ \mathrm{MHz}. \qquad (125)$$

Although the threshold frequency turns out to be rather high, an acoustic experiment seems possible.

7. Conclusions

We have shown that even very weak absorption leads to radical topological changes in wave properties in the vicinity of degenerate directions. We emphasize that these effects exist due to a combination of absorption with the anisotropy of crystals, whereas absorption in isotropic media results in a trivial attenuation of the intensity of wave fields.

We have derived Eqns (14), which, with the correspondence relations (12) and (13), are a universal tool for describing the features of wave parameters both in the acoustics and in the optics of absorptive crystals, in particular, in the vicinity of a conical degeneracy. A unified analysis based on these equations gave a new insight into the wave phenomena being studied in optics and in acoustics and demonstrated not only their similarity but also their difference. We note that some of the subtle topological effects discussed above were theoretically described for the first time.

This primarily applies to all the results presented in Sections 4 and 5. Most of the results on distributions of elliptic polarization fields presented in Section 4 are new. In Section 5, we also obtained some new results in the theory of conical refraction in absorptive crystals. We have shown that this phenomenon exists not only on a wedge edge, as was established previously [11, 12, 16], but also in the whole region of propagation directions of waves in the vicinity of spit axes, where the polarization ellipticity is not small. In addition, we have for the first time described the kinematic features of the motion of ray velocities $\mathbf{s}_\alpha$ over the universal refraction cone and established an exact relation between azimuthal angles of the precession of polarization vectors and the corresponding velocities $\mathbf{s}_\alpha$. In optics, we for the first time considered the general case of an arbitrary anisotropy of a crystal. The theory of refraction has been developed in terms of ray velocities (in [11], the analysis was performed in terms of Umov–Poynting vectors for rhombic crystals only).

Finally, we emphasize that we are not merely dealing here with the mathematical elegance of describing the topological behavior of electromagnetic and elastic waves in absorptive crystals. Numerical estimates performed in Section 6 have shown that the effects under study can be experimentally observed in both optics and acoustics.

Acknowledgments

The authors thank T R Volk and A F Konstantinova for the useful consultations and D A Bessonov for her help in constructing figures.

References

1. Landau L D, Lifshitz E M *Electrodynamics of Continuous Media* (Oxford: Pergamon Press, 1984) [Translated from Russian: *Elektrodinamika Sploshnykh Sred* (Moscow: Nauka, 1982)]
2. Fedorov F I *Optika Anizotropnykh Sred* (Optics of Anisotropic Media) (Minsk: Izd. AN BSSR, 1958); *Optika Anizotropnykh Sred* (Optics of Anisotropic Media) (Moscow: URSS, 2004)
3. Fedorov F I *Teoriya Girotropii* (Theory of Gyrotropy) (Minsk: Nauka i Tekhnika, 1976)
4. Chen H C *Theory of Electromagnetic Waves: a Coordinate-Free Approach* (New York: McGraw-Hill, 1983)
5. Landau L D, Lifshitz E M *Theory of Elasticity* (Oxford: Pergamon Press, 1986) [Translated from Russian: *Teoriya Uprugosti* (Moscow: Nauka, 1987)]

6. Fedorov F I *Theory of Elastic Waves in Crystals* (New York: Plenum Press, 1968) [Translated from Russian: *Teoriya Uprugikh Voln v Kristallakh* (Moscow: Nauka, 1965)]
7. Sirotin Yu I, Shaskolskaya M P *Fundamentals of Crystal Physics* (Moscow: Mir Publ., 1982) [Translated from Russian: *Osnovy Kristallofiziki* (Moscow: Nauka, 1975)]
8. Goncharenko A M, Grum-Grzhimailo S V, Fedorov F I *Kristallografiya* **9** 589 (1964)
9. Lyubimov V N, in *Proc. Intern. Workshop on Dissipation in Physical Systems, Borkow, Poland, 1995*; *Zeszyty Naukowe Politech. Swietokrzyskiej Kielce Poland Mech.* **59** 77 (1995)
10. Berry M V, Dennis M R *Proc. R. Soc. Lond. A* **459** 1261 (2003)
11. Alshits V I, Lyubimov V N *JETP* **98** 870 (2004) [*Zh. Eksp. Teor. Fiz.* **125** 999 (2004)]
12. Alshits V I, Lyubimov V N, in *Proc. Second Workshop on Dissipation in Physical Systems, Borkow, Poland, 1997*; *Zeszyty Naukowe Politech. Swietokrzyskiej Kielce Poland Mech.* **66** 15 (1998)
13. Shuvalov A L, Chadwick P *Phil. Trans. R. Soc. Lond. A* **355** 155 (1997)
14. Shuvalov A L, Scott N H *Q. J. Mech. Appl. Math.* **52** 405 (1999)
15. Shuvalov A L, Scott N H *Acta Mech.* **140** 1 (2000)
16. Alshits V I, Lyubimov V N *JETP* **113** 659 (2011) [*Zh. Eksp. Teor. Fiz.* **140** 755 (2011)]
17. Al'shits V I, Sarychev A V, Shuvalov A L *Sov. Phys. JETP* **62** 531 (1985) [*Zh. Eksp. Teor. Fiz.* **89** 922 (1985)]
18. Alshits V I, Lyubimov V N, Shuvalov L A *Crystallogr. Rep.* **46** 673 (2001) [*Kristallografiya* **46** 742 (2001)]
19. Goncharenko A M *Kristallografiya* **4** 727 (1959)
20. Joly S et al. *Opt. Express* **17** 19868 (2009)
21. Gupta N et al. *J. Opt.* **13** 055702 (2011)
22. Mikhailichenko Yu P *Vestn. TGPU* (6(69)) 130 (2007)
23. Velichkina T S et al. *Sov. Phys. Usp.* **23** 176 (1980) [*Usp. Fiz. Nauk* **130** 357 (1980)]
24. de Klerk J, Musgrave M J P *Proc. Phys. Soc. B* **68** 81 (1955)
25. Musgrave M J P *Acta Crystallogr.* **10** 316 (1957)
26. Khatkevich A G *Kristallografiya* **7** 916 (1962)
27. Barry P A, Musgrave M J P *Q. J. Mech. Appl. Math.* **32** 205 (1979)
28. Aleksandrov K S, Ryzhova T V *Kristallografiya* **9** 373 (1964)